NeurIPT: Foundation Model for Neural Interfaces

Zitao Fang[1] **Chenxuan Li**[1] **Hongting Zhou**[1] **Shuyang Yu**[2] **Guodong Du**[3]
Ashwaq Qasem[1] **Yang Lu**[4] **Jing Li**[5] **Junsong Zhang**[4*] **Sim Kuan Goh**[1*]
[1]Xiamen University Malaysia [2]Columbia University
[3]The Hong Kong Polytechnic University [4]Xiamen University
[5]Harbin Institute of Technology (Shenzhen)
ait2209071@xmu.edu.my zhangjs@xmu.edu.cn simkuangoh@gmail.com

Abstract

Electroencephalography (EEG) has wide-ranging applications, from clinical diagnosis to brain-computer interfaces (BCIs). With the increasing volume and variety of EEG data, there has been growing interest in establishing foundation models (FMs) to scale up and generalize neural decoding. Despite showing early potential, applying FMs to EEG remains challenging due to substantial inter-subject, inter-task, and inter-condition variability, as well as diverse electrode configurations across recording setups. To tackle these open challenges, we propose **NEURIPT**, a foundation model developed for diverse EEG-based **Neur**al **I**nterfaces with a **P**re-trained **T**ransformer by capturing both homogeneous and heterogeneous spatio-temporal characteristics inherent in EEG signals. Temporally, we introduce Amplitude-Aware Masked Pretraining (AAMP), masking based on signal amplitude rather than random intervals, to learn robust representations across varying signal intensities beyond local interpolation. Moreover, this temporal representation is enhanced by a Progressive Mixture-of-Experts (PMoE) architecture, where specialized expert subnetworks are progressively introduced at deeper layers, adapting effectively to the diverse temporal characteristics of EEG signals. Spatially, NeurIPT leverages the 3D physical coordinates of electrodes, enabling effective transfer of embedding across varying EEG settings, and develops Intra-Inter Lobe Pooling (IILP) during fine-tuning to efficiently exploit regional brain features. Empirical evaluations across eight downstream BCI datasets, via fine-tuning, demonstrated NeurIPT consistently achieved state-of-the-art performance, highlighting its broad applicability and robust generalization. Our work pushes forward the state of FMs in EEG and offers insights into scalable and generalizable neural information processing systems. Our project is available at this https URL.

1 Introduction

Electroencephalography (EEG) has been widely adopted as a proxy for brain activity and dynamics, due to its non-invasiveness, portability, and high temporal resolution for real-time monitoring [1]. EEG facilitates investigations into brain function, assists in neurological diagnoses [2], provides objective biomarkers for cognitive and affective states [3], and enables the development of brain-computer interfaces (BCIs) [4]. The growing availability of large-scale EEG datasets (spanning diverse populations, recording configurations, and experimental paradigms) has spurred the development of a wide range of computational approaches, including machine learning and deep learning models (CNN [5], RNN [6], GNN [7], Transformers [8]) for learning representations. However, these models are often tailored to specific tasks and settings, limiting their generalizability and cross-setting applicability. Hence, a paradigm shift is necessary to establish generalizable models that can effectively leverage

*Corresponding authors.

39th Conference on Neural Information Processing Systems (NeurIPS 2025).

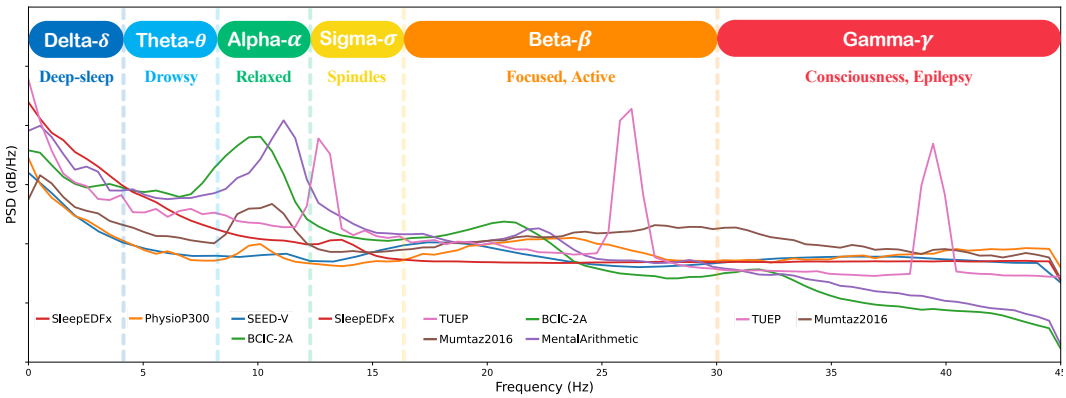

Figure 1: Spectrograms of the nine EEG datasets reveal both homogeneous and heterogeneous spectral patterns, with some datasets showing higher power spectral density (PSD) in specific EEG frequency bands. Thus, they demand neural representations capable of adapting to input variability.

EEG signals across diverse setups and settings, including inter-subject variability, differences between healthy and patients, electrode configurations, and variations in cognitive or behavioral tasks.

Recent advances in foundation models (FMs), large-scale neural architectures pre-trained using transformers on diverse and unlabeled datasets through self-supervised learning [9], followed by fine-tuning on downstream datasets, have demonstrated remarkable success in natural language processing (NLP) and computer vision (CV). In NLP, models [10] such as Claude, DeepSeek, Gemini, GPT, and Llama, pre-trained on massive text corpora, have learned general-purpose representations that transfer effectively to a wide range of downstream tasks [11]. Similarly, pre-trained Vision Transformers (ViTs) [12], Masked Autoencoder (MAE) [13] have become foundational components in modern CV pipelines. These developments highlight the potential of FMs to produce robust, transferable representations of both images and language. Building on this progress, multimodal large language models (MLLMs) (e.g., SORA [14]) further extend these capabilities by integrating information across multiple data modalities, such as text, images, and audio. Hence, it is intriguing to investigate FMs' generalizability to brain signals by developing EEG-based FMs.

Initial efforts to develop foundation models (FMs) for neural decoding showed early promise. BENDR [15] adapted techniques from language modeling to learn compressed representations of raw data signals, enabling the model to generalize across different tasks and datasets. EEG2Vec [16] learned generative-discriminative representations for emotion classification tasks. BIOT [17] addressed the challenges of cross-dataset EEG learning by tokenizing EEG signals into fixed-length segments, accommodating variable-length sequences and mismatched channels. By learning from diverse biosignal datasets, improved performance can be achieved in tasks such as seizure detection. To encode EEG signals into discrete tokens, LaBraM [18] introduced a neural tokenizer with vector-quantized spectrum prediction, facilitating the pretraining of transformers to predict masked segments and enhancing the model's ability to learn from large-scale EEG data. NeuroLM [19] proposed a universal multi-task foundation model that bridged the gap between language and EEG signals. Treating EEG as a foreign language, NeuroLM adopted a text-aligned neural tokenizer and leveraged large language models (LLMs) to perform multi-task learning across various EEG-

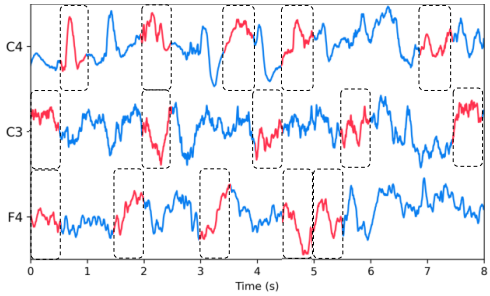

(a) BERT-like random masking.

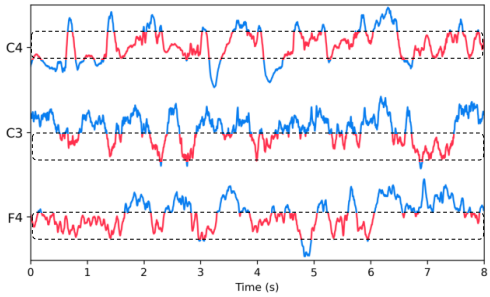

(b) Amplitude-aware masking.

Figure 2: BERT-like random masking v.s. our proposed amplitude-aware masking.

related tasks. EEGPT [20] introduced a dual self-supervised learning approach for feature alignment, capturing spatio-temporal representations in EEG data. This method enhanced the model's ability to learn robust features that generalized across different tasks and datasets. CBraMod [21] presented a criss-cross transformer architecture designed to model spatial and temporal dependencies separately in EEG signals from diverse datasets, facilitating linear probing for fine-tuning on numerous downstream tasks. These methods provided evidence of the applicability of FMs for EEG.

Despite the encouraging preliminary findings, current foundation model (FM) methods for EEG have largely adopted pretraining strategies from language and time-series domains without accounting for several unique properties of EEG. First, existing positional encodings treat electrode channels as interchangeable and ignore their physical three-dimensional arrangement, losing critical spatial relationships, which can significantly impair transferability. Second, prevalent masked pretraining strategies are typically based on randomly masking contiguous signal segments like BERT [22], unintentionally guiding the model toward local interpolation rather than meaningful global representation learning, as illustrated in Figure 2. Third, conventional neural architectures rely heavily on fully connected layers or global pooling mechanisms when fine-tuned to downstream tasks and thus do not explicitly utilize regional brain features. Finally, due to the diversity and complexity of EEG data patterns, ranging from slow-wave oscillations during sleep to rapid spikes during seizures [23], models must be capable of adaptively capturing heterogeneous temporal dynamics recorded in diverse setups. The diverse spectral patterns are shown in Figure 1. Addressing these challenges is critical to fully realizing the potential of foundation models for EEG.

To address the aforementioned challenges, we introduce NEURIPT, a novel EEG foundation model developed to learn robust and generalizable representations across diverse BCI applications. Our NEURIPT include: (i) 3D-Aligned Spatial Encoding, a flexible positional encoding scheme that integrates the actual three-dimensional coordinates of EEG electrodes, enabling seamless adaptation across varying electrode montages without re-training; (ii) Amplitude-Aware Masked Pretraining (AAMP), a novel masking strategy guided by EEG signal amplitude rather than random intervals, shown in Figure 2, compelling the model to capture underlying EEG patterns with amplitude serves as a proxy for signal energy instead of trivial local interpolations; (iii) Progressive Mixture-of-Experts (PMoE), an architectural innovation wherein the number of specialized subnetworks increases with model depth, effectively accommodating diverse temporal EEG patterns; and (iv) Intra-Inter Lobe Pooling (IILP), a spatial aggregation method that performs hierarchical pooling within and across brain lobes, leveraging distinctive regional brain features for downstream tasks. Empirically, NEURIPT achieves consistent state-of-the-art performance across eight diverse EEG benchmarks, including seizure detection, cognitive state decoding, sleep stage classification etc., summarized in Figure 5. Our comprehensive evaluations highlight NEURIPT 's enhanced scalability, improved robustness to spatial and temporal variations, and progress toward building truly universal EEG representation models. These findings mark an advancement for foundation models in EEG and offer practical insights for future neural interface development.

The main contributions of this paper are summarized as follows:

1. We propose NEURIPT, a foundation model developed for EEG-based neural interfaces, designed to learn robust and generalizable representations by capturing the intrinsic spatio-temporal heterogeneity of EEG signals across diverse settings.
2. Temporally, we introduce Amplitude-Aware Masked Pretraining (AAMP), which masks segments based on signal amplitude rather than random intervals, enabling the model to learn robust features across varying signal intensities. In addition, we design a Progressive Mixture-of-Experts (PMoE) architecture that adaptively introduces specialized experts at deeper layers to capture diverse temporal dynamics in EEG.
3. Spatially, NEURIPT incorporates the 3D physical coordinates of electrodes for embedding, facilitating spatial generalization across datasets with varying sensor montages. During fine-tuning, we introduce Intra-Inter Lobe Pooling (IILP) to explicitly model and leverage region-specific brain activity patterns for downstream tasks.
4. We conducted extensive empirical evaluations on eight benchmark BCI datasets. NEURIPT consistently achieved state-of-the-art performance, demonstrating strong generalization and broad applicability across diverse EEG-based tasks.

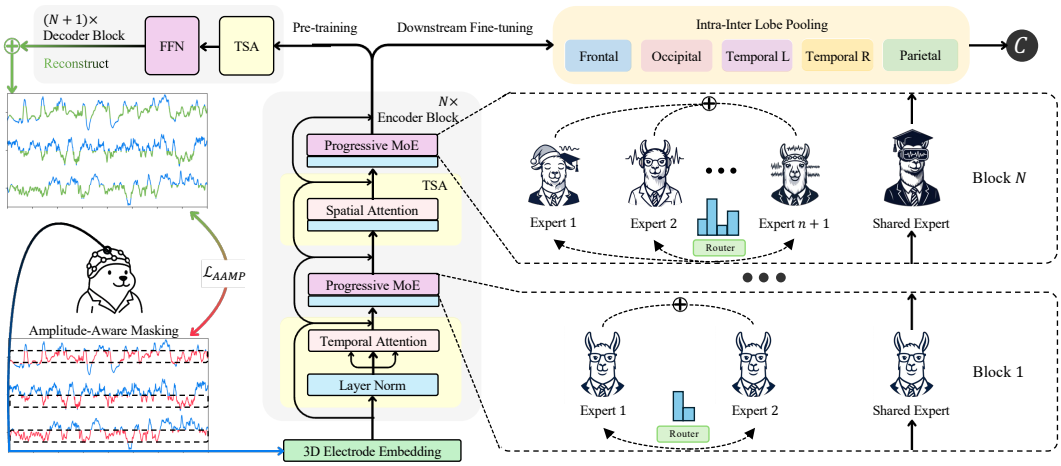

Figure 3: Overview of our **NEURIPT**, which comprises Amplitude-Aware Masked Pretraining (AAMP), 3D Electrode Embedding, Progressive Mixture-of-Experts (PMoE), and Intra-Inter Lobe Pooling (IILP) for fine-tuning. See Figure 4 for details on the IILP module.

2 Method

The framework of NEURIPT is illustrated in Figure 3. In Section 2.1, we provided the details on how NEURIPT integrates spatial and temporal EEG representations by embedding 3D spatial electrode coordinates and employing Amplitude-Aware Masking to enhance self-supervised learning. Subsequently, Section 2.2 describes our Progressive Mixture-of-Experts architecture to dynamically manage EEG variations, complemented by Intra-Inter Lobe Pooling to effectively capture regional brain features for downstream tasks.

2.1 Embedding Spatial Context into Temporal Representations

We pretrain our NEURIPT using self-supervised learning to learn robust representations of EEG signals across diverse setups and settings, without relying on annotations or incorporating any downstream EEG task data. Specifically, given a set of unannotated EEG dataset $\mathcal{D}^{(u)} = \left\{\mathbf{x}^{(i)}\right\}_{i=1}^{N}$, where each sample $\mathbf{x}^{(i)} \in \mathbb{R}^{T\times D}$ represents multivariate EEG signals with T time steps and D electrode channels.

3D Electrode Embedding This is designed to leverage the three-dimensional spatial relationships among EEG electrodes, which are typically arranged according to the international 10–20 electrode placement system. Specifically, for the d-th electrode channel positioned at (x_d, y_d, z_d), we encode its three spatial coordinates separately and concatenate them as follows:

$$PE_d^{(s)} = \text{Concat}\big(PE_x\left(x_d\right), PE_y\left(y_d\right), PE_z\left(z_d\right)\big). \tag{1}$$

Each coordinate embedding uses a sinusoidal function defined as $PE_\alpha(pos)_{2j} = \sin(pos \cdot 10000^{-2j/d_\alpha})$ and $PE_\alpha(pos)_{2j+1} = \cos(pos \cdot 10000^{-2j/d_\alpha})$, where $\alpha \in \{x, y, z\}$ denotes the spatial axes, pos represents the position along the corresponding spatial coordinate, j indexes the embedding dimensions, and $d_\alpha = d_{model}/3$ is the dimensionality of the embedding for axis α.

Building upon pixel-level embeddings in CV [12], we adopt single-point embeddings to preserve temporal details and effectively capture sharp spikes crucial for brain activity analysis. We represent each EEG sample as a collection of data points $\mathbf{x}^{(i)} = \{x_{t,d}^{(i)} \mid 1 \le t \le T, 1 \le d \le D\}$, each point is then embedded with both temporal and spatial information:

$$\mathbf{s}_{t,d}^{(i)} = \mathbf{E}\mathbf{x}^{(i)} + PE^{(t)} + PE^{(s)}. \tag{2}$$

Here, $\mathbf{E} \in \mathbb{R}^{d_{model}}$ denotes a learnable linear projection vector, $PE^{(t)}$ represents temporal positional encoding following the sinusoidal formulation from Vaswani et al. [9]. After embedding, the encoder

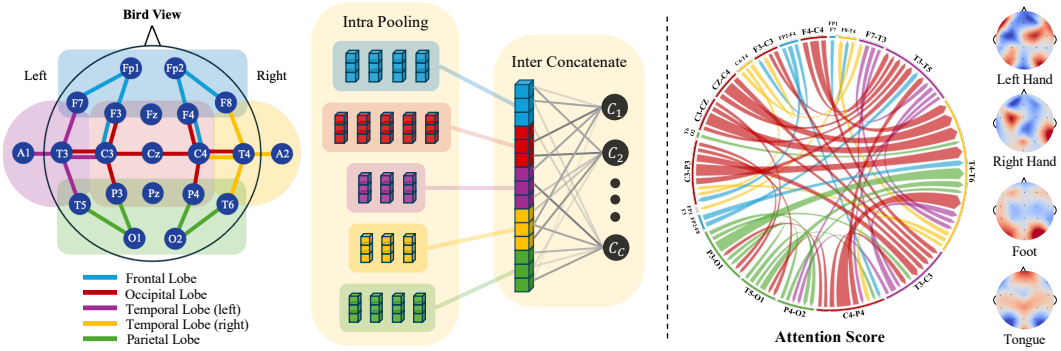

Figure 4: (Left) Intra-Inter Lobe Pooling (IILP) leverages regional brain features during fine-tuning. (Right) Visualization of attention scores from the temporal attention module and analysis of Pearson correlation between class logits and channel perturbation using Gaussian multiplicative noise. Note that colors in the right panel correspond to the brain regions depicted on the left.

input is represented as follows:

$$\mathbf{S}^{enc} = \left\{ \mathbf{s}_{t,d}^{(i)} \middle| t = 1, \ldots, T, d = 1, \ldots, D \right\}, \tag{3}$$

where each vector $\mathbf{s}_{t,d}^{(i)}$ encapsulates both spatial and temporal features, which are crucial for capturing EEG dynamics in subsequent modeling stages. Both temporal and spatial encodings natively support varying temporal lengths T and spatial dimensions D, enabling seamless adaptation to diverse EEG electrode placement systems, such as the 10-05 and 10-20 standards, without additional convolutional components or padding as used in EEGPT [20] and CBraMod [21]. This design is also naturally consistent with the proposed AAMP method introduced below.

Amplitude-Aware Masked Pretraining (AAMP) Self-supervised learning techniques like BERT [22] and MAE [13], which reconstruct randomly masked data, have shown promising results in multivariate time series (MTS) [15, 18, 20]. However, random masking often degrades to simple interpolation between unmasked points in time series data [24], thereby limiting the extraction of meaningful structural representations. To address this, we propose a novel Amplitude-Aware Masking Pretraining (AAMP) approach, explicitly designed to capture more informative features while avoiding mere interpolation, illustrated in Figure 2. After obtaining the embedding array $\mathbf{S}$, we generate our Amplitude-Aware Masking:

$$\mathcal{M} = \left\{ \mathbb{1}\{x_{t,d}^{(i)} \in [\mathcal{L}_d, \mathcal{U}_d]\} \mid t = 1, \ldots, T, d = 1, \ldots, D \right\}, \tag{4}$$

where the interval $[\mathcal{L}_d, \mathcal{U}_d]$ covers $T \cdot \mathcal{P}$ points, centered around the $\xi_d^{(i)} \cdot T$-th point in $sorted(\mathbf{x}_d^{(i)})$. Specifically, probability $\mathcal{P}$ denotes the masking ratio and $\xi_d^{(i)} \sim \mathcal{U}(0, 1)$ is a randomly sampled percentile for dimension d of data instance i. Subsequently, we derive the EEG embedding $\mathbf{S}$, partitioned into the masked set $\mathbf{S}^{\mathcal{M}} = \{\mathbf{s}_{t,d} | m_{t,d} = 1\}$ and the unmasked set $\mathbf{S}^{\mathcal{U}} = \{\mathbf{s}_{t,d} | m_{t,d} = 0\}$ according to the corresponding $\mathbf{s}_{t,d}$ and $m_{t,d}$.

Hierarchical Attention Modules In complex MTS tasks, i.e., EEG signals processing, capturing both temporal and spatial dimensions is significant [21, 25]. To effectively extract these spatio-temporal characteristics at multiple granularities, we adopt Crossformer [26] as part of our backbone architecture, which hierarchically captures alternating temporal and spatial dependencies by using `TSA` module. Further implementation details of our modified Crossformer are provided in Appendix C.1.

Specifically, our hierarchical attention model comprises an encoder $\mathbb{ENC}_{\theta_E}$ and a decoder $\mathbb{DEC}_{\theta_D}$, each equipped with trainable parameters θ_E and θ_D, respectively. These components jointly capture spatio-temporal relationships and reconstruct masked portions of the input data as follows:

$$\hat{\mathbf{x}} = \mathbb{DEC}_{\theta_d}\left(\mathbb{ENC}_{\theta_e}\left(\mathbf{S}^{enc}\right), \mathbf{S}^{dec}\right), \tag{5}$$

and the decoder input $\mathbf{S}^{dec}$ is formulated as:

$$\mathbf{S}^{dec} = \mathbf{E}\left((1 - \mathcal{M}) \odot \mathbf{x}^{(i)}\right) + PE_t^{(t)} + PE_d^{(s)}. \tag{6}$$

The encoder $\mathbb{ENC}_{\theta_e}$ processes the unmasked input $\mathbf{S}^{\mathcal{U}}$ to extract meaningful features while setting the attention scores of the masked set $\mathbf{S}^{\mathcal{M}}$ to zero, thereby preventing unintended access to masked tokens. Thereafter, the decoder $\mathbb{DEC}_{\theta_d}$ reconstructs the signals in $\mathbf{S}^{dec}$ through a specific `[mask]` token, leveraging both the encoder outputs and unmasked signals enriched by comprehensive positional information. We then optimize the parameters θ_E and θ_D by minimizing the ℓ_p-norm reconstruction loss:

$$\mathcal{L}_{\text{AAMP}}(\theta_E, \theta_D) = \frac{1}{n}\left(\sum_{i=1}^{n} \|\mathbf{x}^{(i)} - \hat{\mathbf{x}}^{(i)}\|^p\right)^{1/p}. \tag{7}$$

2.2 Integrating Temporal Dynamics into Spatial Representations

EEG signals exhibit complex, heterogeneous information across various frequency bands, transient events, and even inevitable artifacts, making their representations challenging for a single feed-forward network (FFN). To address this, we leverage a Progressive Mixture-of-Experts (PMoE) architecture, enabling distinct sub-networks as specialized experts to capture specific EEG features, combined with a shared expert to ensure stable generalization. Subsequently, we fine-tune with Intra-Inter Lobe Pooling (IILP), which effectively captures cross-channel connectivity patterns.

Progressive Mixture-of-Experts (PMoE) Given $\hat{\mathbf{Z}}^l \in \mathbb{R}^{T\times D\times d_{model}}$, the output after the attention layer and subsequent layer normalization, a gating mechanism computes token-level routing weights:

$$g^l = \textit{TopKSoftmax}(\text{Router}^{(l)}(\hat{\mathbf{Z}}^l)), \quad \sum_{e=1}^{E_l} g_e^l = 1, \tag{8}$$

where E_l denotes number of experts at the l-th encoder layer and each expert e applies its private sub-network $Y_e^l = \text{FFN}_e^{(l)}(\hat{\mathbf{Z}}^l)$. Introduced by [27], *TopKSoftmax* applies the *softmax* function exclusively to the top-k logits, representing the sparse activation that serves to save computation. These representations are aggregated through gating weights g and further produced the output of transformer block l:

$$\texttt{PMoE}^{(l)}(\hat{\mathbf{Z}}^l) = \sum_{e=1}^{E_l} g_e^l \odot Y_e^l + \text{FFN}_{shared}^{(l)}(\hat{\mathbf{Z}}^l), \tag{9}$$

$$\mathbf{Z}^l = \texttt{PMoE}^{(l)}(\hat{\mathbf{Z}}^l) + \tilde{\mathbf{Z}}^l, \tag{10}$$

where $\odot$ denotes element-wise multiplication, FFN_{shared} denotes the shared expert, and $\tilde{\mathbf{Z}}^l$ denotes the residual connection from the attention output. Then we incorporate an auxiliary loss $\mathcal{L}_{\text{aux}}$ to encourage balanced expert utilization and robust routing behavior [27]. Please refer to Appendix C.1 and C.3 for more details about specific architecture and MoE, respectively.

The shared expert captures generalizable patterns, while the progressively introduced experts handle increasingly specialized signal features [28], effectively adapting to the inherent complexity and variability of EEG signals.

Finetuning with Intra-Inter Lobe Pooling (IILP) Following the pretraining phase, we performed fine-tuning using downstream labeled datasets $\mathcal{D}^{(l)} = \left\{\left(\mathbf{x}^{(j)}, \mathbf{y}^{(j)}\right)\right\}_{j=1}^{n}$ comprising n instances. Each instance $\mathbf{x}^{(j)} \in \mathbb{R}^{T\times D}$ is associated with a class label $\mathbf{y}^{(j)} \in \mathcal{C} := \{1, \ldots, C\}$, indicating the downstream classification category.

To better capture EEG functional connectivity patterns while suppressing redundant information across channels, we propose IILP, a two-step pooling strategy, *Intra-lobe Pooling* followed by *Inter-lobe Concatenation*, illustrated in Figure 4. Given an encoder block output $\mathbf{Z}^{enc,l} \in \mathbb{R}^{T\times D\times d_{model}}$, where T, D, and d_{model} denote the temporal length, number of EEG channels, and embedding dimension, respectively.

We first average-pool Z^{enc} along the temporal axis to aggregate information from all time steps:

$$\widetilde{\mathbf{V}}_d^l = \frac{1}{T}\sum_{t=1}^{T} \mathbf{Z}_{t,d}^{enc,l}, \quad d = 1, \ldots, D. \tag{11}$$

Intra-lobe Pooling. We partition EEG channels into n functional brain lobes, such as frontal and occipital lobes, denoted as $\mathcal{P} = \{P_1, \ldots, P_n\}$. To suppress redundancy within each channel group P, we compute lobe-level embeddings by averaging corresponding channel embeddings:

$$V_k^l = \frac{1}{|P_k|} \sum_{d \in P_k} \widetilde{\mathbf{V}}_d^l, \quad k = 1, \ldots, n. \tag{12}$$

Inter-lobe Concatenation. To leverage discriminative features across different brain lobes, we concatenate the lobe embeddings into a joint representation:

$$v^l = \text{concat}\big(V_1^l, \ldots, V_n^l\big), \tag{13}$$

where $v^l \in \mathbb{R}^{nd_{model}}$ indicates the aggregation vector for encoder block l. Repeating the above IILP process across all encoder blocks and stacking the results yields the final representation:

$$v = \text{concat}\big(v^1, \ldots, v^L\big), \tag{14}$$

where L is the number of encoder blocks. Finally, we use a multilayer perceptron as the classifier on the representation obtained at different granularities to predict the task-specific class from the set $\mathcal{C}$.

3 Experiments

3.1 Pre-training

Datasets NEURIPT is pre-trained using more than 2,000 hours of data collected from public datasets, with the eight downstream datasets explicitly excluded. For more details on pre-training datasets, please refer to Appendix E.1.

Preprocessing To ensure a fair comparison, we follow the data pre-processing pipeline in CBraMod [21]. EEG recordings with a total duration less than 5 minutes were removed, and we discarded the first and last minute of each remaining session to mitigate boundary artifacts. Signals were re-referenced using 20 bipolar channels in the canonical "double banana" montage (e.g., FP1–F7, F7–T3, ..., P4–O2). For further details on preprocessing, please refer to Appendix E.1.2.

Settings We implemented NEURIPT using Python 3.9.19 and PyTorch 2.3.0 with CUDA 12.1 and cuDNN 8902. Pre-training stage was trained using the AdamW optimizer combined with the OneCycle learning rate strategy [29] (upper learning rate 3e-4, divided factor 25, final divided factor 1e4, and cosine annealing strategy). The pre-training process was conducted for approximately 400K steps, employing an effective batch size of 480 and bfloat16 mixed-precision training on eight NVIDIA GeForce RTX 4090 GPUs. For more details on implementation settings and hyperparameters, please refer to Appendix D and Table 13.

Table 1: Overview of downstream BCI tasks and datasets.

BCI Tasks	Datasets	Rate	Channels Used	Duration	Samples	Label
I. Mental Stress Detection	MentalArithmetic	500Hz	20	5s	1,707	2-class
II. Mental Disorder Diagnosis	Mumtaz2016	256Hz	20	5s	6,963	2-class
III. P300	PhysioNetP300	2048Hz	20	2s	21,179	2-class
IV. Sleep Staging	Sleep-EDFx	100Hz	2	30s	457,652	5-class
V. Emotion Recognition	SEED-V	1000Hz	20	1s	115,001	5-class
VI. Motor Imagery Task	BCIC-IV-2A	250Hz	16	4s	5,184	4-class
VII. Abnormal Detection	TUAB	250Hz	20	10s	409,455	2-class
VIII. Event Type Classification	TUEV	250Hz	20	5s	112,491	6-class

3.2 Downstream BCI Tasks

BCI Tasks and Datasets To comprehensively assess the effectiveness of NEURIPT, we evaluated it across eight diverse BCI datasets spanning multiple downstream task categories. A summary of all tasks and corresponding datasets is provided in Table 1 and detailed in Appendix E.2.1. To ensure fair comparison, we adopt the same data processing protocols as CBraMod [21]. Additional details on each downstream dataset and preprocessing pipeline are presented in Appendix E.2.

Baselines and Metrics All the baselines and metrics are detailed in Appendix D.2.

Table 2: The results of NEURIPT on various datasets. Figure 5 demonstrates the visual comparison.

Datasets	Methods	Balanced Accuracy	Cohen's Kappa / AUC-PR	Weighted F1 / AUROC
MentalArithmetic	BIOT [NeurIPS23] [17]	68.75	60.04	75.36
	LaBraM [ICLR24] [18]	69.09	59.99	77.21
	CBraMod [ICLR25] [21]	72.56	62.67	79.05
	NEURIPT (Ours)	**86.46** (+13.90)	**78.27** (+15.60)	**91.11** (+12.06)
Mumtaz2016	BIOT [NeurIPS23] [17]	93.58	97.36	97.58
	LaBraM [ICLR24] [18]	94.09	97.98	97.82
	CBraMod [ICLR25] [21]	95.60	99.23	99.21
	NEURIPT (Ours)	**98.03** (+2.43)	**99.81** (+0.58)	**99.79** (+0.58)
*PhysioP300	BENDR [15]	61.14	22.27	65.88
	BIOT [NeurIPS23] [17]	54.85	9.68	53.08
	LaBraM [ICLR24] [18]	64.77	29.35	70.68
	EEGPT [NeurIPS24] [20]	65.02	29.99	71.68
	NEURIPT (Ours)	**67.31** (+2.29)	**34.26** (+4.27)	**76.83** (+5.15)
Sleep-EDFx	BENDR [15]	66.55	66.59	75.07
	BIOT [NeurIPS23] [17]	66.22	64.61	74.15
	LaBraM [ICLR24] [18]	67.71	67.10	75.92
	EEGPT [NeurIPS24] [20]	69.17	68.57	76.54
	NEURIPT (Ours)	**70.47** (+1.30)	**77.57** (+9.00)	**87.39** (+10.85)
SEED-V	BIOT [NeurIPS23] [17]	38.37	22.61	38.56
	LaBraM [ICLR24] [18]	39.76	23.86	39.74
	CBraMod [ICLR25] [21]	40.91	25.69	41.01
	NEURIPT (Ours)	**41.04** (+0.13)	**26.29** (+0.60)	**41.58** (+0.57)
BCIC-IV-2A	BIOT [NeurIPS23] [17]	47.48	29.97	46.07
	LaBraM [ICLR24] [18]	48.69	31.59	47.58
	CBraMod [ICLR25] [21]	51.38	35.18	49.84
	NEURIPT (Ours)	**55.04** (+3.66)	**40.04** (+4.86)	**53.76** (+3.92)
TUAB	BIOT [NeurIPS23] [17]	79.59	87.92	88.15
	LaBraM [ICLR24] [18]	82.58	92.04	91.62
	EEGPT [NeurIPS24] [20]	79.83	-	87.18
	NeuroLM [ICLR25] [21]	79.69	72.19	78.84
	CBraMod [ICLR25] [21]	82.89	**92.58**	**92.27**
	NEURIPT (Ours)	**82.93** (+0.04)	90.40 (-2.18)	89.49 (-2.78)
TUEV	BIOT [NeurIPS23] [17]	52.81	52.73	74.92
	LaBraM [ICLR24] [18]	66.16	67.45	83.29
	EEGPT [NeurIPS24] [20]	62.32	63.51	81.87
	NeuroLM [ICLR25] [21]	46.79	45.70	73.59
	CBraMod [ICLR25] [21]	66.71	67.72	83.42
	NEURIPT (Ours)	**67.61** (+0.90)	**69.70** (+1.98)	**84.28** (+0.86)

3.3 Main Results

We present a comparative analysis of our method against baselines across eight downstream datasets in Table 2, with the best results highlighted in bold. Moreover, we report the performance difference between our method and the best-performing baseline. Compared to the baselines, our method generally outperforms them on the majority of datasets, with the exception of Cohen's Kappa and AUROC metrics on TUAB. Notably, our method achieves significant improvements on the Mental Arithmetic, PhysioP300, and BCIC-IV-2A datasets. While the performance gains are smaller on other datasets, they remain consistent, demonstrating the robustness and general applicability of our approach. Extensive empirical evaluations on eight benchmark BCI datasets consistently demonstrate strong generalization and broad applicability across diverse EEG-based tasks. Appendix E.2 gives the specific experimental results on each task, including experimental configuration and results analysis.

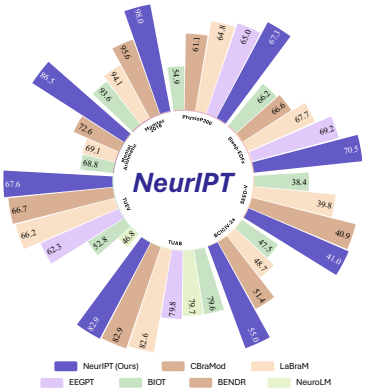

Figure 5: Models performance on various BCI downtream tasks.

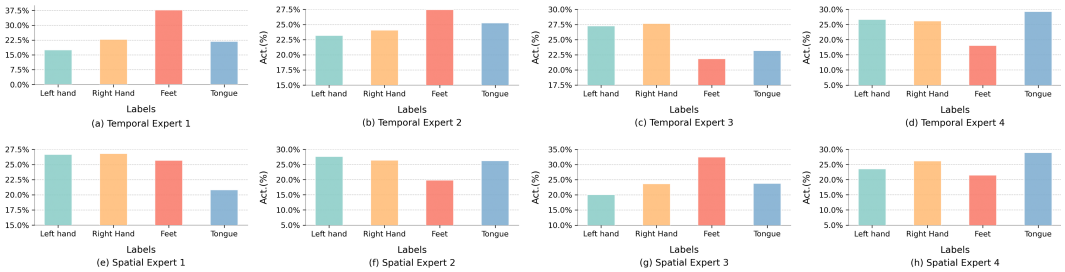

Figure 6: Analysis of expert participation (temporal and spatial) when EEG data from different classes of the BCIC-IV-2A dataset is input to the model.

3.4 Additional Results and Analysis

Analysis of Spatial Relationships between EEG Channels To analyze spatial relationships, we presented in Figure 4 the attention scores from a spatial attention head, along with an analysis of the Pearson correlation between class logits and channel perturbations using Gaussian multiplicative noise. The attention score visualization reveals both inter- and intra-lobe interactions, which aligns with the strengths of IILP. From the perturbation analysis, we observe contralateral activation patterns in channels C3 and C4 for hand-related tasks, and a more symmetrical pattern for foot and tongue movements, in line with findings from the existing study [30]. Refer to Figure 8 and 16 in Appendix G for more visualization about the attention score and Pearson correlation in various datasets.

Analysis of Progressive Mixture-of-Experts (PMoE) We analyzed how temporal and spatial experts in the PMoE architecture contribute to the prediction of the four classes in the BCIC-IV-2A dataset, with the statistics presented in Figure 6. It is observed that different classes engage varying numbers of experts, with some classes receiving attention from a larger number of experts. Refer to Figure 9-15 in Appendix G for more expert contributions across different datasets.

Table 3: Different MoE strategies across various datasets.

MoE Strategies	No. of Experts	TUEV	MentalArithmetic	Mumtaz2016	SEED-V	PhysioP300	BCIC-2A
w/o Expert	[0, 0, 0, 0, 0, 0]	65.83	72.92	93.41	39.14	64.53	44.44
Uniform	[4, 4, 4, 4, 4, 4]	65.91	70.49	95.00	39.33	65.66	41.93
Shrinking	[6, 4, 4, 4, 0, 0]	65.80	73.96	93.08	39.21	65.99	**44.62**
Progressive (Ours)	[0, 0, 2, 4, 4, 6]	**68.94**	**75.69**	**97.07**	**39.34**	**66.58**	44.01

Table 4: Different PMoE configurations across various datasets.

PMoE Configurations	TUEV	MentalArithmetic	Mumtaz2016	SEED-V	PhysioP300	BCIC-2A
[0,0,2,4,4,6]	**68.94**	75.69	97.07	39.34	66.58	**44.01**
[0,0,2,3,4,5]	67.87	**76.39**	96.81	**39.88**	66.34	41.58
[0,0,2,4,6,8]	66.41	75.69	96.57	39.11	**67.70**	41.15
[0,0,3,6,9,12]	66.08	74.83	**97.15**	39.35	66.63	38.19

Ablation of MoE Strategies and PMoE Configurations Tables 3 and 4 show the ablation results of MoE strategies and PMoE configurations, respectively. When varying the number of experts across layers, our PMoE, which increases the number of experts with depth, consistently outperforms both the non-MoE baseline, the uniform-expert variant, and the shrinking MoE variant, where the number of experts decreases with depth. The alternative configs in Table 4 also yield competitive performance, which suggests that the effectiveness of the PMoE approach stems from its inherent progressive strategy, rather than relying on any specific expert allocation, demonstrating robustness across diverse progressive configurations.

Table 5: Different pooling strategies across various datasets.

Pooling Strategies	TUEV	MentalArithmetic	Mumtaz2016	SEED-V	PhysioP300	BCIC-2A
w/o Pooling	62.33	75.69	78.21	38.90	**67.82**	45.14
Mean Pooling	64.74	79.51	96.22	37.62	66.72	37.24
Hemispheres	64.45	81.94	97.82	39.22	67.11	43.49
Coronal	68.77	73.26	96.99	39.35	66.98	43.75
Sagittal	67.21	80.21	91.41	39.42	65.66	45.31
IILP (Ours)	**68.94**	**86.46**	**98.03**	**41.04**	67.31	**55.04**

Table 6: Ablation study on each individual component in NEURIPT. Results are based on models trained from scratch, without the time-intensive pre-training stage.

3D PE	PMoE	IILP	TUEV	MentalArithmetic	Mumtaz2016	SEED-V	BCIC-IV-2A
✗	✗	✗	51.80	73.36	91.83	37.82	32.64
✓	✗	✗	59.64	73.61	86.07	38.54	40.19
✗	✓	✗	52.79	74.65	85.58	37.82	33.59
✗	✗	✓	59.10	73.96	91.55	35.66	37.15
✓	✓	✗	62.33	**75.69**	78.21	38.90	**45.14**
✓	✗	✓	65.83	72.92	93.41	39.14	44.44
✗	✓	✓	67.72	74.65	96.56	35.03	37.59
✓	✓	✓	**68.94**	**75.69**	**97.07**	**39.34**	44.01

Ablation of Pooling Strategies We compared our Intra-Inter Lobe Pooling (IILP) with no pooling as well as pooling strategies based on coronal, sagittal, and hemispheric brain region groupings. The results are presented in Table 5, demonstrating the consistent effectiveness and superiority of IILP.

Ablation of Each Individual Component The ablation in Table 6 demonstrates that performance across datasets generally improves with the inclusion of each component, achieving peak accuracy when all components are combined. Notably, the IILP module significantly enhances results on the TUEV and Mumtaz2016 datasets. This improvement is presumably because epilepsy and depression classification tasks require capturing distinctive regional signal variations across different brain areas.

For BCIC-IV-2A, which primarily involves motor imagery tasks and was recorded using EEG channels located centrally with limited coverage of other brain lobes, we observed a performance decline when the 3D PE component was excluded. This suggests that motor imagery tasks are particularly sensitive to spatial information, as further supported by our channel perturbation analysis in Figure 4. Given the low-data scenario (BCIC-IV-2A includes only nine subjects), explicitly encoding physical spatial relationships becomes especially important. Moreover, excluding only IILP may degrade performance due to incomplete brain lobe coverage, limiting the model's utilization of lobe-specific information, yet incorporating it during pretraining enhances generalization (see Table 5).

Table 7: Different activation functions for EEG FMs (trained from scratch, same as Table 6).

Activation Function	TUEV	MentalArithmetic	Mumtaz2016	SEED-V	PhysioP300	BCIC-2A
ReLU	64.01	73.96	96.98	38.37	66.29	**47.31**
GELU	64.02	73.61	**97.14**	38.69	64.38	46.35
SwiGLU	**68.94**	**75.69**	97.07	**39.34**	**66.58**	44.01

Exploration of Activation Function for EEG Foundation Models (FMs) Different datasets exhibited distinct preferences (Table 7): ReLU performed particularly well on BCIC-2A, whereas GELU achieved competitive results on Mumtaz2016. Nonetheless, SwiGLU demonstrated the most consistent performance across multiple downstream tasks, indicating its robustness in FMs for EEG data.

Further Results and Analysis For further results and analysis, please refer to Appendix B.

4 Conclusion

This study introduces NEURIPT, a foundation model established for diverse EEG-based neural interfaces, overcoming the challenges in learning generalizable spatio-temporal representations of EEG signals from diverse sources. Temporally, we propose Amplitude-Aware Masked Pretraining (AAMP), which selects masked segments based on signal amplitude rather than random intervals, encouraging the model to capture robust features across varying signal intensities and avoiding reliance on local interpolation. This is complemented by a Progressive Mixture-of-Experts (PMoE) architecture, which progressively incorporates specialized expert subnetworks at deeper layers to better adapt to the temporal variability inherent in EEG data. Spatially, NEURIPT utilizes the 3D physical coordinates of electrodes to support transferable embeddings across different EEG configurations and introduces Intra-Inter Lobe Pooling (IILP) during fine-tuning to effectively leverage region-specific brain activity. Comprehensive evaluations on eight benchmark EEG datasets demonstrate NEURIPT 's consistent state-of-the-art performance and strong generalization. These findings highlight NEURIPT's potential as a scalable foundation model for EEG, moving toward universal neural decoding systems.

Acknowledgments

This work was supported in part by the Ministry of Higher Education Malaysia through the Fundamental Research Grant Scheme (FRGS/1/2023/ICT02/XMU/02/1); National Natural Science Foundation of China (62476070, 62376233); Shenzhen Science and Technology Program (JCYJ20241202123503005, GXWD20231128103232001, ZDSYS20230626091203008, KQTD20240729102154066); Department of Science and Technology of Guangdong (2024A1515011540); Natural Science Foundation of Fujian Province (2024J09001); Collaborative Innovation Platform Project for Fuzhou-Xiamen-Quanzhou National Independent Innovation Demonstration Zone (2022-P-028); Xiaomi Young Talents Program; Xiamen University Malaysia Research Fund (XMUMRF/2024-C13/IECE/0049, XMUMRF/2024-C14/IECE/0055).

References

[1] Neethu Robinson, Ravikiran Mane, Tushar Chouhan, and Cuntai Guan. Emerging trends in bci-robotics for motor control and rehabilitation. *Current Opinion in Biomedical Engineering*, 20:100354, 2021. ISSN 2468-4511. doi: https://doi.org/10.1016/j.cobme.2021.100354. URL https://www.sciencedirect.com/science/article/pii/S2468451121000945. 1

[2] Iyad Obeid and Joseph Picone. The temple university hospital eeg data corpus. *Frontiers in Neuroscience*, 10:196, 2016. doi: 10.3389/fnins.2016.00196. URL https://doi.org/10.3389/fnins.2016.00196. 1, 27, 30

[3] Wei Liu, Jie-Lin Qiu, Wei-Long Zheng, and Bao-Liang Lu. Comparing recognition performance and robustness of multimodal deep learning models for multimodal emotion recognition. *IEEE Transactions on Cognitive and Developmental Systems*, 14(2):715–729, 2022. doi: https://doi.org/10.1109/TCDS.2021.3071170. 1, 26, 29

[4] Michael Tangermann, Klaus-Robert Müller, Ad Aertsen, Niels Birbaumer, Christoph Braun, Clemens Brunner, Robert Leeb, Carsten Mehring, K. J. Miller, Gernot R. Müller-Putz, Guido Nolte, Gert Pfurtscheller, Hubert Preissl, Gerwin Schalk, Alois Schlögl, Carmen Vidaurre, Stephan Waldert, and Benjamin Blankertz. Review of the bci competition iv. *Frontiers in Neuroscience*, 6:55, 2012. doi: https://doi.org/10.3389/fnins.2012.00055. 1, 26, 30

[5] Sim Kuan Goh, Hussein A. Abbass, Kay Chen Tan, Abdullah Al-Mamun, Nitish Thakor, Anastasios Bezerianos, and Junhua Li. Spatio–spectral representation learning for electroencephalographic gait-pattern classification. *IEEE Transactions on Neural Systems and Rehabilitation Engineering*, 26(9):1858–1867, 2018. doi: 10.1109/TNSRE.2018.2864119. URL https://ieeexplore.ieee.org/document/8428659. 1, 17

[6] Hongli Li, Man Ding, Ronghua Zhang, and Chunbo Xiu. Motor imagery eeg classification algorithm based on cnn-lstm feature fusion network. *Biomedical Signal Processing and Control*, 72:103342, 2022. ISSN 1746-8094. doi: https://doi.org/10.1016/j.bspc.2021.103342. 1, 17, 24, 27, 28, 29, 30, 31

[7] Siyi Tang, Jared Dunnmon, Khaled Kamal Saab, Xuan Zhang, Qianying Huang, Florian Dubost, Daniel Rubin, and Christopher Lee-Messer. Self-supervised graph neural networks for improved electroencephalographic seizure analysis. In *International Conference on Learning Representations (ICLR)*, 2022. URL https://openreview.net/forum?id=k9bx1EfHI_-. 1, 17

[8] Yonghao Song, Xueyu Jia, Lie Yang, and Longhan Xie. Transformer-based spatial-temporal feature learning for eeg decoding. *arXiv preprint arXiv:2106.11170*, 2021. URL https://arxiv.org/abs/2106.11170. 1, 17, 24, 27, 28, 29, 30, 31

[9] Ashish Vaswani, Noam Shazeer, Niki Parmar, Jakob Uszkoreit, Llion Jones, Aidan N Gomez, Ł ukasz Kaiser, and Illia Polosukhin. Attention is all you need. In I. Guyon, U. Von Luxburg, S. Bengio, H. Wallach, R. Fergus, S. Vishwanathan, and R. Garnett, editors, *Advances in Neural Information Processing Systems*, volume 30. Curran Associates, Inc., 2017. URL https://proceedings.neurips.cc/paper_files/paper/2017/file/3f5ee243547dee91fbd053c1c4a845aa-Paper.pdf. 2, 4, 17, 19, 21

[10] Tianchen Gao, Jiashun Jin, Zheng Tracy Ke, and Gabriel Moryoussef. A comparison of deepseek and other llms. *arXiv preprint arXiv:2502.03688*, 2025. URL https://arxiv.org/abs/2502.03688. 2, 17

[11] Zitao Fang, Guodong Du, Shuyang Yu, Yifei Guo, Yiwei Zhang, Yiyao Cao, Jing Li, Ho-Kin Tang, and Sim Kuan Goh. To see a world in a spark of neuron: Disentangling multi-task interference for training-free model merging. In *Proceedings of the 2025 Conference on Empirical Methods in Natural Language Processing (EMNLP)*. Association for Computational Linguistics, 2025. URL https://arxiv.org/abs/2503.05320. 2

[12] Duy Kien Nguyen, Mido Assran, Unnat Jain, Martin R. Oswald, Cees G. M. Snoek, and Xinlei Chen. An image is worth more than 16x16 patches: Exploring transformers on individual pixels. In *The Thirteenth International Conference on Learning Representations (ICLR)*, 2025. URL https://openreview.net/forum?id=tjNf0L8QjR. 2, 4

[13] Kaiming He, Xinlei Chen, Saining Xie, Yanghao Li, Piotr Dollár, and Ross Girshick. Masked autoencoders are scalable vision learners. In *Proceedings of the IEEE/CVF Conference on Computer Vision and Pattern Recognition (CVPR)*, pages 16000–16009, June 2022. doi: 10.1109/CVPR52688.2022.01553. URL https://ieeexplore.ieee.org/document/9879206. 2, 5

[14] Yixin Liu, Kai Zhang, Yuan Li, Zhiling Yan, Chujie Gao, Ruoxi Chen, Zhengqing Yuan, Yue Huang, Hanchi Sun, Jianfeng Gao, et al. Sora: A review on background, technology, limitations, and opportunities of large vision models. *arXiv preprint arXiv:2402.17177*, 2024. URL https://arxiv.org/abs/2402.17177. 2

[15] Demetres Kostas, Stéphane Aroca-Ouellette, and Frank Rudzicz. Bendr: Using transformers and a contrastive self-supervised learning task to learn from massive amounts of eeg data. *Frontiers in Human Neuroscience*, 15:653659, 2021. doi: 10.3389/fnhum.2021.653659. URL https://doi.org/10.3389/fnhum.2021.653659. 2, 5, 8, 17, 24, 28, 29

[16] David Bethge, Philipp Hallgarten, Tobias Grosse-Puppendahl, Mohamed Kari, Lewis L Chuang, Ozan Özdenizci, and Albrecht Schmidt. Eeg2vec: Learning affective eeg representations via variational autoencoders. In *2022 IEEE International Conference on Systems, Man, and Cybernetics (SMC)*, pages 3150–3157. IEEE, 2022. URL https://ieeexplore.ieee.org/document/9945517. 2, 17

[17] Chaoqi Yang, M Westover, and Jimeng Sun. Biot: Biosignal transformer for cross-data learning in the wild. In A. Oh, T. Naumann, A. Globerson, K. Saenko, M. Hardt, and S. Levine, editors, *Advances in Neural Information Processing Systems (NeurIPS)*, volume 36, pages 78240–78260. Curran Associates, Inc., 2023. URL https://proceedings.neurips.cc/paper_files/paper/2023/file/f6b30f3e2dd9cb53bbf2024402d02295-Paper-Conference.pdf. 2, 8, 17, 24, 27, 28, 29, 30, 31

[18] Wei-Bang Jiang, Li-Ming Zhao, and Bao-Liang Lu. Large brain model for learning generic representations with tremendous EEG data in BCI. In *The Twelfth International Conference on Learning Representations (ICLR)*, 2024. URL https://openreview.net/forum?id=QzTpTRVtrP. 2, 5, 8, 17, 19, 24, 27, 28, 29, 30, 31

[19] Weibang Jiang, Yansen Wang, Bao liang Lu, and Dongsheng Li. NeuroLM: A universal multi-task foundation model for bridging the gap between language and EEG signals. In *The Thirteenth International Conference on Learning Representations (ICLR)*, 2025. URL https://openreview.net/forum?id=Io9yFt7XH7. 2, 17, 24, 31

[20] Guagnyu Wang, Wenchao Liu, Yuhong He, Cong Xu, Lin Ma, and Haifeng Li. Eegpt: Pretrained transformer for universal and reliable representation of eeg signals. In A. Globerson, L. Mackey, D. Belgrave, A. Fan, U. Paquet, J. Tomczak, and C. Zhang, editors, *Advances in Neural Information Processing Systems*, volume 37, pages 39249–39280. Curran Associates, Inc., 2024. URL https://proceedings.neurips.cc/paper_files/paper/2024/file/4540d267eeec4e5dbd9dae9448f0b739-Paper-Conference.pdf. 3, 5, 8, 17, 24, 28, 29, 31

[21] Jiquan Wang, Sha Zhao, Zhiling Luo, Yangxuan Zhou, Haiteng Jiang, Shijian Li, Tao Li, and Gang Pan. CBramod: A criss-cross brain foundation model for EEG decoding. In *The Thirteenth International Conference on Learning Representations (ICLR)*, 2025. URL https://openreview.net/forum?id=NPNUHgHF2w. 3, 5, 7, 8, 17, 24, 27, 28, 29, 30, 31

[22] Jacob Devlin, Ming-Wei Chang, Kenton Lee, and Kristina Toutanova. BERT: Pre-training of deep bidirectional transformers for language understanding. In Jill Burstein, Christy Doran, and Thamar Solorio, editors, *Proceedings of the 2019 Conference of the North American Chapter of the Association for Computational Linguistics: Human Language Technologies, Volume 1 (Long and Short Papers)*, pages 4171–4186, Minneapolis, Minnesota, June 2019. Association for Computational Linguistics. doi: 10.18653/v1/N19-1423. URL https://aclanthology.org/N19-1423/. 3, 5, 22

[23] Chaoqi Yang, Danica Xiao, M Brandon Westover, and Jimeng Sun. Self-supervised eeg representation learning for automatic sleep staging. *arXiv preprint arXiv:2110.15278*, 2021. URL https://arxiv.org/abs/2110.15278. 3, 24, 27, 28, 29, 30, 31

[24] Dongwei Jiang, Wubo Li, Ruixiong Zhang, Miao Cao, Ne Luo, Yang Han, Wei Zou, Kun Han, and Xiangang Li. A further study of unsupervised pretraining for transformer based speech recognition. In *ICASSP 2021 - 2021 IEEE International Conference on Acoustics, Speech and Signal Processing (ICASSP)*, pages 6538–6542, 2021. doi: 10.1109/ICASSP39728.2021.9414539. URL https://ieeexplore.ieee.org/document/9414539. 5

[25] Yong Liu, Tengge Hu, Haoran Zhang, Haixu Wu, Shiyu Wang, Lintao Ma, and Mingsheng Long. itransformer: Inverted transformers are effective for time series forecasting. In *The Twelfth International Conference on Learning Representations (ICLR)*, 2024. URL https://openreview.net/forum?id=JePfAI8fah. 5

[26] Yunhao Zhang and Junchi Yan. Crossformer: Transformer utilizing cross-dimension dependency for multivariate time series forecasting. In *The Eleventh International Conference on Learning Representations (ICLR)*, 2023. URL https://openreview.net/forum?id=vSVLM2j9eie. 5, 21

[27] Noam Shazeer, *Azalia Mirhoseini, *Krzysztof Maziarz, Andy Davis, Quoc Le, Geoffrey Hinton, and Jeff Dean. Outrageously large neural networks: The sparsely-gated mixture-of-experts layer. In *International Conference on Learning Representations (ICLR)*, 2017. URL https://openreview.net/forum?id=B1ckMDqlg. 6, 22

[28] Ka Man Lo, Zeyu Huang, Zihan Qiu, Zili Wang, and Jie Fu. A closer look into mixture-of-experts in large language models. In Luis Chiruzzo, Alan Ritter, and Lu Wang, editors, *Findings of the Association for Computational Linguistics: NAACL 2025*, pages 4427–4447, Albuquerque, New Mexico, April 2025. Association for Computational Linguistics. ISBN 979-8-89176-195-7. URL https://aclanthology.org/2025.findings-naacl.251/. 6

[29] Leslie N Smith and Nicholay Topin. Super-convergence: Very fast training of neural networks using large learning rates. In *Artificial intelligence and machine learning for multi-domain operations applications*, volume 11006, pages 369–386. SPIE, 2019. 7

[30] Yang An, Hak Keung Lam, and Sai Ho Ling. Multi-classification for eeg motor imagery signals using data evaluation-based auto-selected regularized fbcsp and convolutional neural network. *Neural Computing and Applications*, 35(16):12001–12027, June 2023. ISSN 1433-3058. doi: https://doi.org/10.1007/s00521-023-08336-z. 9

[31] Brendan Z. Allison, Jing Jin, Yu Zhang, and Xingyu Wang. A four-choice hybrid p300/ssvep bci for improved accuracy. *Brain-Computer Interfaces*, 1(1):17–26, 2014. doi: 10.1080/2326263X.2013.869003. 17

[32] Chao Jiang, Yingjie Li, Yingying Tang, and Cuntai Guan. Enhancing eeg-based classification of depression patients using spatial information. *IEEE Transactions on Neural Systems and Rehabilitation Engineering*, 29:566–575, 2021. doi: 10.1109/TNSRE.2021.3059429. URL https://ieeexplore.ieee.org/document/9354645. 17

[33] Qingshan She, Chenqi Zhang, Feng Fang, Yuliang Ma, and Yingchun Zhang. Multisource associate domain adaptation for cross-subject and cross-session eeg emotion recognition. *IEEE Transactions on Instrumentation and Measurement*, 72:1–12, 2023. doi: 10.1109/TIM.2023.3277985. URL https://ieeexplore.ieee.org/document/10129888. 17

[34] Zhongke Gao, Weidong Dang, Xinmin Wang, Xiaolin Hong, Linhua Hou, Kai Ma, and Matjaž Perc. Complex networks and deep learning for eeg signal analysis. *Cognitive Neurodynamics*, 15(3):369–388, 2021. ISSN 1871-4099. doi: 10.1007/s11571-020-09626-1. URL https://doi.org/10.1007/s11571-020-09626-1. 17

[35] Lukas Wolf, Ard Kastrati, Martyna B Plomecka, Jie-Ming Li, Dustin Klebe, Alexander Veicht, Roger Wattenhofer, and Nicolas Langer. A deep learning approach for the segmentation of electroencephalography data in eye tracking applications. In Kamalika Chaudhuri, Stefanie Jegelka, Le Song, Csaba Szepesvari, Gang Niu, and Sivan Sabato, editors, *Proceedings of the 39th International Conference on Machine Learning (ICML)*, volume 162 of *Proceedings of Machine Learning Research*, pages 23912–23932. PMLR, 17–23 Jul 2022. URL https://proceedings.mlr.press/v162/wolf22a.html. 17

[36] Jin Xie, Jie Zhang, Jiayao Sun, Zheng Ma, Liuni Qin, Guanglin Li, Huihui Zhou, and Yang Zhan. A transformer-based approach combining deep learning network and spatial-temporal information for raw eeg classification. *IEEE Transactions on Neural Systems and Rehabilitation Engineering*, 30:2126–2136, 2022. doi: 10.1109/TNSRE.2022.3194600. URL https://ieeexplore.ieee.org/document/9845479. 17

[37] Soyiba Jawed, Ibrahima Faye, and Aamir Saeed Malik. Deep learning-based assessment model for real-time identification of visual learners using raw eeg. *IEEE Transactions on Neural Systems and Rehabilitation Engineering*, 32:378–390, 2024. doi: 10.1109/TNSRE.2024.3351694. URL https://ieeexplore.ieee.org/document/10387266. 17

[38] Aaqib Saeed, David Grangier, Olivier Pietquin, and Neil Zeghidour. Learning from heterogeneous eeg signals with differentiable channel reordering. In *ICASSP 2021 - 2021 IEEE International Conference on Acoustics, Speech and Signal Processing (ICASSP)*, pages 1255–1259, 2021. doi: https://doi.org/10.1109/ICASSP39728.2021.9413712. 17

[39] Aaqib Saeed, David Grangier, and Neil Zeghidour. Contrastive learning of general-purpose audio representations. In *ICASSP 2021 - 2021 IEEE International Conference on Acoustics, Speech and Signal Processing (ICASSP)*, pages 3875–3879, 2021. doi: https://doi.org/10.1109/ICASSP39728.2021.9413528. 17

[40] Daya Guo, Dejian Yang, Haowei Zhang, Junxiao Song, Peiyi Wang, et al. Deepseek-r1 incentivizes reasoning in llms through reinforcement learning. *Nature*, 645:633–638, 2025. doi: 10.1038/s41586-025-09422-z. URL https://www.nature.com/articles/s41586-025-09422-z. 17, 21

[41] An Yang, Anfeng Li, Baosong Yang, Beichen Zhang, Binyuan Hui, Bo Zheng, Bowen Yu, Chang Gao, Chengen Huang, Chenxu Lv, et al. Qwen3 technical report. *arXiv preprint arXiv:2505.09388*, 2025. 17, 21

[42] Ruibin Xiong, Yunchang Yang, Di He, Kai Zheng, Shuxin Zheng, Chen Xing, Huishuai Zhang, Yanyan Lan, Liwei Wang, and Tie-Yan Liu. On layer normalization in the transformer architecture. In *Proceedings of the 37th International Conference on Machine Learning (ICML)*, ICML'20. JMLR.org, 2020. URL https://proceedings.mlr.press/v119/xiong20b.html. 21

[43] Dan Hendrycks and Kevin Gimpel. Gaussian error linear units (gelus). *arXiv preprint arXiv:1606.08415*, 2016. URL https://arxiv.org/abs/1606.08415. 21

[44] Noam Shazeer. Glu variants improve transformer. *arXiv preprint arXiv:2002.05202*, 2020. URL https://arxiv.org/abs/2002.05202. 21

[45] Hugo Touvron, Louis Martin, Kevin Stone, Peter Albert, Amjad Almahairi, Yasmine Babaei, Nikolay Bashlykov, Soumya Batra, Prajjwal Bhargava, Shruti Bhosale, et al. Llama 2: Open foundation and fine-tuned chat models. *arXiv preprint arXiv:2307.09288*, 2023. URL https://arxiv.org/abs/2307.09288. 21

[46] Aaron Grattafiori, Abhimanyu Dubey, Abhinav Jauhri, Abhinav Pandey, Abhishek Kadian, Ahmad Al-Dahle, Aiesha Letman, Akhil Mathur, Alan Schelten, Alex Vaughan, et al. The llama 3 herd of models. *arXiv preprint arXiv:2407.21783*, 2024. URL https://arxiv.org/abs/2407.21783. 21

[47] An Yang, Baosong Yang, Binyuan Hui, Bo Zheng, Bowen Yu, Chang Zhou, Chengpeng Li, Chengyuan Li, Dayiheng Liu, Fei Huang, et al. Qwen2 technical report. *arXiv preprint arXiv:2407.10671*, 2024. URL https://arxiv.org/abs/2407.10671. 21

[48] Qwen, An Yang, Baosong Yang, Beichen Zhang, Binyuan Hui, Bo Zheng, Bowen Yu, Chengyuan Li, Dayiheng Liu, Fei Huang, et al. Qwen2.5 technical report. *arXiv preprint arXiv:2412.15115*, 2025. URL https://arxiv.org/abs/2412.15115. 21

[49] Aixin Liu, Bei Feng, Bing Xue, Bingxuan Wang, Bochao Wu, Chengda Lu, Chenggang Zhao, Chengqi Deng, Chenyu Zhang, Chong Ruan, et al. Deepseek-v3 technical report. *arXiv preprint arXiv:2412.19437*, 2024. URL https://arxiv.org/abs/2412.19437. 21

[50] Tri Dao. Flashattention-2: Faster attention with better parallelism and work partitioning. In *The Twelfth International Conference on Learning Representations (ICLR)*, 2024. URL https://openreview.net/forum?id=mZn2Xyh9Ec. 21, 23

[51] Zhengzhuo Xu, Ruikang Liu, Shuo Yang, Zenghao Chai, and Chun Yuan. Learning imbalanced data with vision transformers. In *2023 IEEE/CVF Conference on Computer Vision and Pattern Recognition (CVPR)*, pages 15793–15803, 2023. doi: 10.1109/CVPR52729.2023.01516. 22

[52] Vernon J Lawhern, Amelia J Solon, Nicholas R Waytowich, Stephen M Gordon, Chou P Hung, and Brent J Lance. Eegnet: a compact convolutional neural network for eeg-based brain–computer interfaces. *Journal of Neural Engineering*, 15(5):056013, jul 2018. doi: https://doi.org/10.1088/1741-2552/aace8c. 24, 27, 28, 29, 30, 31

[53] Yonghao Song, Qingqing Zheng, Bingchuan Liu, and Xiaorong Gao. Eeg conformer: Convolutional transformer for eeg decoding and visualization. *IEEE Transactions on Neural Systems and Rehabilitation Engineering*, 31:710–719, 2023. doi: https://doi.org/10.1109/TNSRE.2022.3230250. 24, 27, 28, 29, 30, 31

[54] Jin Jing, Wendong Ge, Shenda Hong, Marta Bento Fernandes, Zhen Lin, Chaoqi Yang, Sungtae An, Aaron F Struck, Aline Herlopian, Ioannis Karakis, et al. Development of expert-level classification of seizures and rhythmic and periodic patterns during eeg interpretation. *Neurology*, 100(17):e1750–e1762, 2023. doi: https://doi.org/10.1212/WNL.0000000000207127. 24, 27, 28, 29, 30, 31

[55] Wei Yan Peh, Yuanyuan Yao, and Justin Dauwels. Transformer convolutional neural networks for automated artifact detection in scalp eeg. In *2022 44th Annual International Conference of the IEEE Engineering in Medicine and Biology Society (EMBC)*, pages 3599–3602, 2022. doi: https://doi.org/10.1109/EMBC48229.2022.9871916. 24, 27, 28, 29, 30, 31

[56] Arman Savran, Koray Ciftci, Guillame Chanel, Javier Cruz Mota, Luong Hong Viet, Bülent Sankur, Lale Akarun, Alice Caplier, and Michele Rombaut. Emotion detection in the loop from brain signals and facial images. In *Summer Workshop on Multimodal Interfaces (eINTERFACE 2006)*, pages 69–80, 2006. URL https://www.isca-archive.org/einterface_2006/savran06_einterface.html. 25

[57] Matthew D. Luciw, Ewa Jarocka, and Benoni B. Edin. Multi-channel EEG recordings during 3,936 grasp and lift trials with varying weight and friction. *Scientific Data*, 1(1):140047, 2014. ISSN 2052-4463. doi: 10.1038/sdata.2014.47. URL https://doi.org/10.1038/sdata.2014.47. 25

[58] Margaux Perrin, Emmanuel Maby, Sébastien Daligault, Olivier Bertrand, and Jérémie Mattout. Objective and subjective evaluation of online error correction during P300-based spelling. *Advances in Human-Computer Interaction*, 2012:578295, 2012. doi: 10.1155/2012/578295. URL https://onlinelibrary.wiley.com/doi/10.1155/2012/578295. 25

[59] G. Schalk, D.J. McFarland, T. Hinterberger, N. Birbaumer, and J.R. Wolpaw. Bci2000: a general-purpose brain-computer interface (bci) system. *IEEE Transactions on Biomedical Engineering*, 51(6):1034–1043, 2004. doi: 10.1109/TBME.2004.827072. URL https://ieeexplore.ieee.org/document/1300799. 25

[60] Logan Trujillo. Raw EEG Data, 2020. URL https://doi.org/10.18738/T8/SS2NHB. 25

[61] Logan T. Trujillo, Candice T. Stanfield, and Ruben D. Vela. The effect of electroencephalogram (eeg) reference choice on information-theoretic measures of the complexity and integration of eeg signals. *Frontiers in Neuroscience*, 11:425, 2017. doi: 10.3389/fnins.2017.00425. URL https://doi.org/10.3389/fnins.2017.00425. 25

[62] Wei-Long Zheng and Bao-Liang Lu. Investigating critical frequency bands and channels for eeg-based emotion recognition with deep neural networks. *IEEE Transactions on Autonomous Mental Development*, 7 (3):162–175, 2015. doi: 10.1109/TAMD.2015.2431497. URL https://doi.org/10.1109/TAMD.2015.2431497. 25

[63] Wei-Long Zheng, Wei Liu, Yifei Lu, Bao-Liang Lu, and Andrzej Cichocki. Emotionmeter: A multimodal framework for recognizing human emotions. *IEEE Transactions on Cybernetics*, 49(3):1110–1122, 2019. doi: 10.1109/TCYB.2018.2797176. URL https://doi.org/10.1109/TCYB.2018.2797176. 25

[64] Wei Liu, Wei-Long Zheng, Ziyi Li, Si-Yuan Wu, Lu Gan, and Bao-Liang Lu. Identifying similarities and differences in emotion recognition with eeg and eye movements among chinese, german, and french people. *Journal of Neural Engineering*, 19(2):026012, mar 2022. doi: 10.1088/1741-2552/ac5c8d. URL https://doi.org/10.1088/1741-2552/ac5c8d. 25

[65] Paolo Detti, Giampaolo Vatti, and Garazi Zabalo Manrique de Lara. Eeg synchronization analysis for seizure prediction: A study on data of noninvasive recordings. *Processes*, 8(7), 2020. ISSN 2227-9717. doi: 10.3390/pr8070846. URL https://doi.org/10.3390/pr8070846. 25

[66] Mastaneh Torkamani-Azar, Sumeyra Demir Kanik, Serap Aydin, and Mujdat Cetin. Prediction of reaction time and vigilance variability from spatio-spectral features of resting-state eeg in a long sustained attention task. *IEEE Journal of Biomedical and Health Informatics*, 24(9):2550–2558, 2020. doi: 10.1109/JBHI.2020.2980056. URL https://doi.org/10.1109/JBHI.2020.2980056. 25

[67] Louis Korczowski, Martine Cederhout, Anton Andreev, Grégoire Cattan, Pedro Luiz Coelho Rodrigues, Violette Gautheret, and Marco Congedo. Brain Invaders calibration-less P300-based BCI with modulation of flash duration Dataset (bi2015a). Research report, GIPSA-lab, July 2019. URL https://hal.science/hal-02172347. 26

[68] G. Buckwalter, S. Chhin, S. Rahman, I. Obeid, and J. Picone. Recent advances in the tuh eeg corpus: Improving the interrater agreement for artifacts and epileptiform events. In *2021 IEEE Signal Processing in Medicine and Biology Symposium (SPMB)*, pages 1–3, 2021. doi: 10.1109/SPMB52430.2021.9672302. URL https://doi.org/10.1109/SPMB52430.2021.9672302. 26

[69] L. Veloso, J. McHugh, E. von Weltin, S. Lopez, I. Obeid, and J. Picone. Big data resources for eegs: Enabling deep learning research. In *2017 IEEE Signal Processing in Medicine and Biology Symposium (SPMB)*, pages 1–3, 2017. doi: 10.1109/SPMB.2017.8257044. URL https://doi.org/10.1109/SPMB.2017.8257044. 26

[70] Vinit Shah, Eva von Weltin, Silvia Lopez, James Riley McHugh, Lillian Veloso, Meysam Golmohammadi, Iyad Obeid, and Joseph Picone. The temple university hospital seizure detection corpus. *Frontiers in Neuroinformatics*, 12:83, 2018. ISSN 1662-5196. doi: 10.3389/fninf.2018.00083. URL https://doi.org/10.3389/fninf.2018.00083. 26

[71] E. von Weltin, T. Ahsan, V. Shah, D. Jamshed, M. Golmohammadi, I. Obeid, and J. Picone. Electroencephalographic slowing: A primary source of error in automatic seizure detection. In *2017 IEEE Signal Processing in Medicine and Biology Symposium (SPMB)*, pages 1–5, 2017. doi: 10.1109/SPMB.2017.8257018. URL https://doi.org/10.1109/SPMB.2017.8257018. 26

[72] Ary L Goldberger, Luis AN Amaral, Leon Glass, Jeffrey M Hausdorff, Plamen Ch Ivanov, Roger G Mark, Joseph E Mietus, George B Moody, Chung-Kang Peng, and H Eugene Stanley. Physiobank, physiotoolkit, and physionet: components of a new research resource for complex physiologic signals. *Circulation*, 101 (23):e215–e220, 2000. doi: https://doi.org/10.1161/01.CIR.101.23.e215. 26, 27

[73] Igor Zyma, Sergii Tukaev, Ivan Seleznov, Ken Kiyono, Anton Popov, Mariia Chernykh, and Oleksii Shpenkov. Electroencephalograms during mental arithmetic task performance. *Data*, 4(1), 2019. ISSN 2306-5729. doi: https://doi.org/10.3390/data4010014. URL https://www.mdpi.com/2306-5729/4/1/14. 26, 27

[74] Wajid Mumtaz. MDD Patients and Healthy Controls EEG Data (New). *figshare*, November 2016. doi: https://doi.org/10.6084/m9.figshare.4244171.v2. URL https://figshare.com/articles/dataset/EEG_Data_New/4244171. 26, 27

[75] Luca Citi, Riccardo Poli, and Caterina Cinel. Documenting, modelling and exploiting p300 amplitude changes due to variable target delays in donchin's speller. *Journal of Neural Engineering*, 7(5):056006, sep 2010. doi: https://doi.org/10.1088/1741-2560/7/5/056006. 26, 28

[76] B. Kemp, A.H. Zwinderman, B. Tuk, H.A.C. Kamphuisen, and J.J.L. Oberye. Analysis of a sleep-dependent neuronal feedback loop: the slow-wave microcontinuity of the eeg. *IEEE Transactions on Biomedical Engineering*, 47(9):1185–1194, 2000. doi: https://doi.org/10.1109/10.867928. 26, 28

A Related Work

Existing literature on EEG-based neural decoding can be broadly categorized according to the evolution from EEG setting-specific models to generalizable foundation models, as outlined below:

A.1 Decoding EEG Signals with Task- and Setup-Specific Models

EEG decoding has evolved from classical BCI pipelines, that develop computational approaches based on the well-known EEG signatures (e.g., P300, event-related (de)synchronization, Steady-State Visual Evoked Potential (SSVEP), etc [31]) to feature engineering and statistical classifiers such as, linear discriminant analysis (LDA), or support vector (SVM), random forest, common spatial pattern (CSP) [5, 32], to more sophisticated machine learning and deep learning models tailored for specific tasks and recording setups. These models are often trained on specific datasets and optimized for particular paradigms, such as motor imagery [32], gait recognition [5], emotion recognition [33], and seizure detection [7], under fixed channel layouts, devices, or recording conditions, building upon prior knowledge of EEG characteristics. Deep learning approaches such as CNN [5], RNN [6], GNN [7], Transformers [8], and their hybrids have been widely applied to model EEG's complex spatiotemporal dynamics using spectrogram, time-frequency representation, and brain connectivity [34].

Recent work has shifted end-to-end learning paradigms that learn representations directly on raw EEG signals [35, 36, 37], reducing the dependence on handcrafted preprocessing. However, these methods still struggle with generalization across subjects, devices, or experimental conditions and require retraining when used in different settings.

A.2 Unified EEG Signal Decoding with Pretrained Foundation Models

Motivated by the success of foundation models in natural language processing (NLP) [9, 10], recent trends in EEG research focus on developing large-scale, pretrained neural architectures that scale up and generalize across diverse EEG tasks, conditions, experimental setups, and subjects. These models are typically pre-trained using self-supervised learning on unlabeled EEG data from varied sources, enabling the extraction of task and subject-invariant representations that can be fine-tuned for a wide range of downstream EEG applications. Broadly, three main lines of approaches have emerged: (i) modeling EEG as a multivariate time series using transformer-based architectures adapted from the speech or time-series domains, such as BENDR [15] and EEG2Vec [16]; (ii) tokenizing continuous EEG signals into discrete tokens to enable large-scale pretraining analogous to language modeling, as in LaBraM [18] and NeuroLM [19]; and (iii) preserving EEG's spatiotemporal structure using specialized architectures that consider both between EEG channels and temporal dynamics from diverse datasets through neural architectural design, exemplified by recent EEG-based FMs, BIOT [17], EEGPT [20], and CBraMod [21]. These FMs reduce the need for task-specific calibration and enhance robustness and scalability in real-world BCI and EEG-based applications. CHARM [38] addressed inconsistent input channels through a learnable channel-level masking approach, and COLA [39] employed contrastive learning rather than masking-based self-supervised pretraining on large-scale audio data. These related works offer valuable complementary perspectives on enhancing EEG modeling.

While these pioneering FMs showed early promise, a few important EEG characteristics are not considered in the current FMs, such as the physical three-dimensional arrangement of electrodes, diverse EEG patterns and intensity across diverse datasets, and brain regional features are not fully taken into account. Moreover, recent successes of Mixture-of-Experts (MoE) [40, 41] based foundation models have demonstrated impressive scalability and generalization in fields like LLMs, by designing a larger network (for more parameters) with sub-networks that are only activated by relevant task (for less computation); however, their application and potential benefits remain largely unexplored in EEG decoding. This work attempts to fill the research gap for developing a robust EEG-based FM.

B Additional Results and Analysis

This section continues from Section 3.4 of the main text and provides further results and analysis.

Table 8: Comparison between different masking strategies (masking ratio: 50%).

Masking Strategy	Bal. Acc.
BERT-style random masking	0.6320
Amplitude-aware masking	**0.6845**

Ablation of Masking Strategies We compare and analyze our proposed amplitude-aware masking pretraining (AAMP) strategy with BERT-style random masking in Table 8. We directly evaluate the pretrained representations by performing a downstream classification task using Support Vector Machine (SVM)[2], aiming to assess the quality of the learned representations obtained during the pretraining stage.[3] Our amplitude-based masking improves 5.25% compared to random masking, proving the effectiveness of masking based on amplitude. Figure 7 illustrates the training loss between to strategies. After 1000 steps, random masking has lower reconstruction loss, demonstrating that random masking is better for learning reconstruction. This implies that the model is better at interpolation under random masking, but ultimately performs poorly in downstream classification tasks. Refer to Figure 18, 19 and 20 of Appendix G for more visualization comparisons.

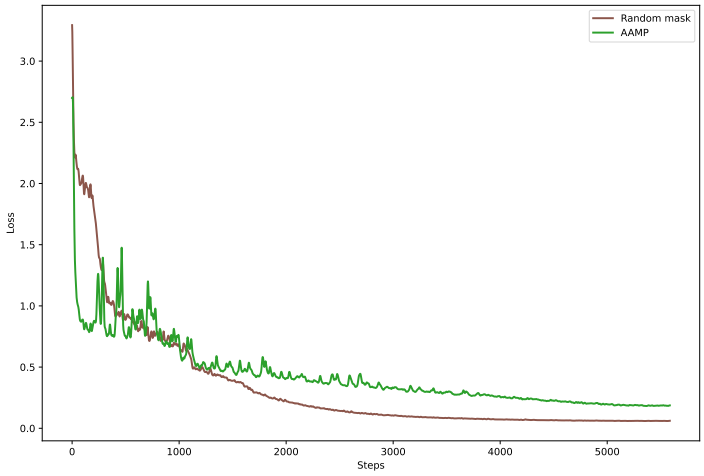

Figure 7: Training loss between different masking strategies.

Analysis of Masking Ratio We then also tested the performance of our AAMP at different masking ratios. As Table 9 shows, SVM works best at a masking ratio of 50%. Figure 17 of Appendix G shows the loss curves for different masking ratios.

Table 9: Performance of NEURIPT with different masking ratios.

Masking Ratio (%)	Bal. Acc.
30	0.5523
40	0.6321
50	**0.6845**
60	0.5596
70	0.5254

[2]For the classification task in Appendix B, we selected the TUEV due to its complexity and variety, consisting of six distinct classes. To manage the computational complexity of SVM, which scales quadratically with the number of data points, we randomly sampled 5000 data points from the training set and 500 data points from the test set, using a fixed random seed (520) to ensure reproducibility. Hyperparameters were optimized via grid search with 5-fold cross-validation on the sampled training data, and the best-performing combination was subsequently evaluated on the test set. Detailed ranges of hyperparameters explored during the grid search are presented in Appendix D.1 and Table 14.

[3]We use smaller models for quick tests. Specifically, we set d_{model} to 256, expert hidden FFN_{expert} to 128, shared expert hidden FFN_{shared} to 256. The rest of the parameters remain the same as the original pre-trained model.

Table 10: Comparison between different masking strategies across diverse downstream tasks.

Datasets	Masking Strategies	Bal. Acc.	Cohen's Kappa	Weighted F1
TUEV	Random Masking	67.35	67.28	83.37
	AAMP (Ours)	**67.61**	**69.70**	**84.28**
MentalArithmetic	Random Masking	84.38	77.89	90.98
	AAMP (Ours)	**86.46**	**78.27**	**91.11**
Mumtaz2016	Random Masking	97.14	**99.84**	**99.84**
	AAMP (Ours)	**98.03**	99.81	99.79
SEED-V	Random Masking	33.89	17.07	33.82
	AAMP (Ours)	**41.04**	**26.29**	**41.58**
PhysioP300	Random Masking	65.64	28.99	72.75
	AAMP (Ours)	**67.31**	**34.26**	**76.83**
Sleep-EDFx	Random Masking	69.68	76.82	87.11
	AAMP (Ours)	**70.47**	**77.57**	**87.39**

Further Ablation of Masking Strategies We analyzed the classification performance in the preceding using SVM classifiers trained directly on representations generated under different masking strategies. Table 10 compares the downstream task performances between BERT-like random masking and our proposed AAMP, further demonstrating the advantages of our method.

Table 11: Different positional encoding strategies across various tasks. Alternative encoding strategies are included: trigonometric functions and 1D learnable embeddings employed by vanilla Transformer [9], and 2D learnable embeddings introduced in LaBraM [18].

Datasets	Encoding Strategies	Bal. Acc.	Cohen's Kappa	Weighted F1
TUEV	Trigonometric Functions	67.72	68.85	84.03
	Learnable 1D	64.78	67.92	83.13
	Learnable 2D	63.81	66.63	82.57
	3D PE (Ours)	**68.94**	**71.55**	**85.17**
MentalArithmetic	Trigonometric Functions	74.65	71.84	83.80
	Learnable 1D	71.53	74.23	83.17
	Learnable 2D	71.52	64.81	80.83
	3D PE (Ours)	**75.69**	**74.37**	**86.83**
Mumtaz2016	Trigonometric Functions	96.56	99.59	99.61
	Learnable 1D	96.63	99.21	99.23
	Learnable 2D	95.56	99.55	99.54
	3D PE (Ours)	**97.07**	**99.83**	**99.84**
SEED-V	Trigonometric Functions	35.03	18.58	35.08
	Learnable 1D	35.52	18.81	34.34
	Learnable 2D	37.40	21.54	37.34
	3D PE (Ours)	**39.34**	**23.93**	**39.67**

Ablation of Positional Encoding Strategies Table 11 presents ablation studies on different position encoding methods. Our proposed 3D PE consistently outperforms both the trigonometric function embedding and the learnable 1D and 2D embeddings, underscoring its effectiveness in explicitly leveraging physical electrode positions inherent in EEG data.

Table 12: Low resource scenario. Metrics are shown as percentages relative to the full-data baseline.

Datasets	Data Used	Bal. Acc.	Cohen's Kappa	Weighted F1
TUEV	1%	64.16	72.44	88.08
	5%	75.39	81.78	91.67
	10%	80.30	88.64	95.75
	100%	100.00	100.00	100.00
Sleep-EDFx	1%	80.97	83.86	91.33
	5%	86.01	79.82	90.41
	10%	92.51	92.74	96.13
	100%	100.00	100.00	100.00

Low Data Scenario The performance of NEURIPT under low-resource scenarios is presented in Table 12. Our approach achieved notable classification accuracy, maintaining performance in the range of $80\% - 90\%$ with merely 10% of the original data, and even with an extremely limited 1% of data, performance remains competitive at $64\% - 80\%$. These results further confirm the robustness of our pretraining strategy and underscore the model's potential in few-shot and low-resource settings.

For the ablation studies in Table 6 and 7 in Section 3.4, due to time and resource constraints, the results presented are based on models trained from scratch, without the time-intensive pre-training stage.

C Additional Methodological Details

C.1 Backbone Architecture

We adopt Crossformer [26] as our backbone architecture, which leverages the TSA (Two-stage attention, including cross-time attention and cross-dimension attention) module to hierarchically capture alternating temporal and spatial dependencies. Additionally, the hierarchical structure of TSA, especially at deeper layers with coarser granularity, significantly reduces sequence lengths and computational demands, enabling efficient resource utilization during large-scale pre-training. Furthermore, we replace the Post-LN with Pre-LN [42] and switch the activation function from GELU [43] to SwiGLU [44] for a more stable training process, aligning with mainstream large language models such as the Llama [45, 46], Qwen [41, 47, 48], and Deepseek [40, 49] series. The mathematical formulation of our modified backbone is as follows:

Temporal Stage After embedding, $\mathbf{S}^{enc} \in \mathbb{R}^{T\times D\times d_{model}}$ is the encoder block $\mathbb{ENC}$'s input, where T and D are the number of time steps and electrode channels, respectively. Consistent with Section 2.2, $\mathbf{Z}^{l-1}$ is the output of the layer $l-1$ and $\bar{\mathbf{Z}}^{l}$ is the input of the layer l after merging. Thus at the first layer, $\mathbf{Z}^0 = \mathbf{S}^{enc}$. For convenience, in the following, we use $\mathbf{Z}_{i,:}$ to denote the vectors of all dimensions at time step i, $\mathbf{Z}_{:,d}$ for those of all time steps in dimension d. In the temporal stage, we directly apply multi-head self-attention MSA to each dimension:

$$\check{\mathbf{Z}}^{time,l} = \texttt{LayerNorm}\left(\bar{\mathbf{Z}}^{l-1}\right) \tag{15}$$

$$\hat{\mathbf{Z}}^{time,l}_{:,d} = \texttt{LayerNorm}\left(\bar{\mathbf{Z}}^{l-1} + \texttt{MSA}\left(\check{\mathbf{Z}}^{time,l}_{:,d}, \check{\mathbf{Z}}^{time,l}_{:,d}, \check{\mathbf{Z}}^{time,l}_{:,d}\right)\right) \tag{16}$$

$$\mathbf{Z}^{time,l} = \texttt{PMoE}^{(l)}_1\left(\hat{\mathbf{Z}}^{time,l}_{:,d}\right) + \tilde{\mathbf{Z}}^{time,l}_{:,d} \tag{17}$$

where $1 \le d \le D$ and LayerNorm denotes pre-layer normalization [42], $\texttt{MSA}(\mathbf{Q}, \mathbf{K}, \mathbf{V})$ denotes the multi-head self-attention layer [9] where $\mathbf{Q}, \mathbf{K}, \mathbf{V}$ serve as queries, keys and values, PMoE denotes the Progressive Mixture-of-Experts introduced in Section 2.2, and $\tilde{\mathbf{Z}}^{time,l}_{:,d}$ denotes the residual connection result from Equation 16 but without LayerNorm. All dimensions $(1 \le d \le D)$ share the same MSA layer. $\mathbf{Z}^{time,l}$ denotes the output of the cross-time stage.

Spatial Stage Similarly to the temporal stage, we also apply the above architecture to each time step:

$$\check{\mathbf{Z}}^{dim,l} = \texttt{LayerNorm}\left(\mathbf{Z}^{time,l}\right) \tag{18}$$

$$\hat{\mathbf{Z}}^{dim,l}_{i,:} = \texttt{LayerNorm}\left(\mathbf{Z}^{time,l} + \texttt{MSA}\left(\check{\mathbf{Z}}^{dim,l}_{i,:}, \check{\mathbf{Z}}^{dim,l}_{i,:}, \check{\mathbf{Z}}^{dim,l}_{i,:}\right)\right) \tag{19}$$

$$\mathbf{Z}^{l} = \texttt{PMoE}^{(l)}_2\left(\hat{\mathbf{Z}}^{dim,l}_{:,d}\right) + \tilde{\mathbf{Z}}^{dim,l}_{:,d} \tag{20}$$

where $1 \le i \le T$ and $\tilde{\mathbf{Z}}^{dim,l}_{:,d}$ denotes the residual connection result from Equation 19 but without LayerNorm. Finally, $\mathbf{Z}^l$ is the output of the entire TSA layer l. Notably, in practice, at the first layer, we split Equation 2 into the following two parts to embed the temporal and spatial information separately:

$$\check{\mathbf{Z}}^{time,1} = \texttt{LayerNorm}\left(\mathbf{Z}^0 + \mathbf{PE}^{(t)}\right) \tag{21}$$

$$\check{\mathbf{Z}}^{dim,1} = \texttt{LayerNorm}\left(\mathbf{Z}^{time,1} + \mathbf{PE}^{(s)}\right) \tag{22}$$

Equations 21, 22 correspond to Equations 15, 18, respectively, and represent special cases at the first layer. Here, multi-head self-attention MSA is implemented through FlashAttention-2 by [50] to achieve faster speeds.

Hierarchical Attention Modules In each encoder layer (except the first layer), every adjacent m_l vectors are merged to produce representations at progressively coarser temporal scales. Then, a TSA layer captures dependencies at this new scale. Formally, the encoder process $\mathbb{ENC}$ for layer l is defined as:

$$\begin{cases} l = 1: & \bar{\mathbf{Z}}^{enc,0} = \mathbf{Z}^{enc,0}, \\ l > 1: & \bar{\mathbf{Z}}^{enc,l}_{i,d} = \mathbf{M}\left[\mathbf{Z}^{enc,l}_{(i-1)m_l+1,d} \cdot \mathbf{Z}^{enc,l}_{(i-1)m_l+2,d} \cdot \cdots \cdot \mathbf{Z}^{enc,l}_{im_l,d}\right], \end{cases} \tag{23}$$

where $1 \leq i \leq \left\lceil \frac{T_{l-1}}{m_l} \right\rceil$, $1 \leq d \leq D$, $\mathbf{Z}^{enc,l}$ denotes the output of the l-th encoder layer, $\mathbf{M} \in \mathbb{R}^{d_{model} \times m_l d_{model}}$ is a learnable matrix for dynamic segment merging, "$\cdot$" denotes the concatenation operation, T_{l-1} denotes the number of segments in layer $l-1$, and if not divisible by m_l, padding is applied to $\mathbf{Z}^{enc,l-1}$ accordingly.

C.2 Additional Masking Strategy

Besides Amplitude-Aware Masking Pretraining (AAMP), we incorporate an additional basic masking strategy proposed in BERT [22]: 80% of the selected tokens are replaced with the `[mask]` token, 10% are replaced with a randomly sampled embedding from a predefined set $\mathbf{S}$ to mitigate overfitting, and the remaining 10% are left unchanged to prevent the model from overly relying on the `[mask]` token.

C.3 Mixture-of-Experts

We incorporate an auxiliary loss consisting of an importance loss $\mathcal{L}^{(l)}_{\text{importance}}$ and a load-balancing loss $\mathcal{L}^{(l)}_{\text{balance}}$ of layer l proposed by Google Brain [27]. This auxiliary loss promotes equitable expert allocation, improving model efficiency and generalization:

$$\mathcal{L}_{\text{aux}} = \sum_{l=1}^{L} \mathcal{L}^{(l)}_{\text{importance}} + \mathcal{L}^{(l)}_{\text{balance}}. \tag{24}$$

C.4 Balanced Binary Cross Entropy

We applied Bal-BCE [51], a logit-adjusted balanced binary cross-entropy loss that has achieved promising results in long-tailed image datasets. Here, we explore similar approaches for imbalanced BCI downstream datasets. Let $\pi_{\mathbf{y}_i} = n_{\mathbf{y}_i}/N$ represent the class distribution for $\mathbf{y}_i$, where the bias term of the logit $\mathbf{z}_{\mathbf{y}_i}$ is given by $\mathcal{B}^{\text{bce}}_{\mathbf{y}_i} = \log \pi_{\mathbf{y}_i} - \log(1 - \pi_{\mathbf{y}_i})$. Based on this logit bias adjustment, the loss function we adopt during the fine-tuning stage is as follows:

$$\mathcal{L}_{\text{Bal-BCE}} = -\sum_{\mathbf{y}_i \in \mathcal{C}} w_i \left[\mathbb{1}(\mathbf{y}_i) \cdot \log \sigma \left(\mathbf{z}_{\mathbf{y}_i} + \mathcal{B}^{\text{bce}}_{\mathbf{y}_i} \right) + (1 - \mathbb{1}(\mathbf{y}_i)) \cdot \log \left(1 - \sigma \left(\mathbf{z}_{\mathbf{y}_i} + \mathcal{B}^{\text{bce}}_{\mathbf{y}_i} \right) \right) \right], \tag{25}$$

where $\mathbb{1}$ is 1 if the condition is true and $\sigma(x) = 1/\left(1 + e^{-x}\right)$ indicates the sigmoid operation.

D Implementation Details

D.1 Hyperparameters and Settings

Table 13: Hyperparameters for NEURIPT pre-training.

	Hyperparameters	Settings
EEG sample	Channels	20
	Data length	256
	Dynamic masking ratio	[20,35,50]
Model Architecture	Input dimension	768
	Output dimension	768
	Feed-forward dimension	768
	Heads	8
	Merge layers	[1,4,1,2,1,2]
PMoE Configuration	Hidden dimension of expert	512
	Shared expert hidden dimension	768
	Encoder expert	[0,2,2,4,4,6]
	Decoder expert	[0,0,0,0,0,0]
	Cross expert	[0,0,0,0,0,0]
	Top-$k\%$	0.5
	Noise std	0.001
	W importance	0.008
	Auxiliary loss weight	0.8
Pre-training	Epochs	40
	Batch size	60
	Dropout	0.1
	Optimizer	AdamW
	Maximum learning rate	3e-4
	Div factor	25
	Final div factor	1e4
	Warm up ratio	0.15
	AdamW (β_1, β_2)	(0.9, 0.98)
	Weight decay	5e-3
	Scheduler	CosineAnnealingLR
	Cosine cycle epochs	40
	Minimal learning rate	1e-5
	Clipping gradient	100
	Weights init	Kaiming normalization
	Seed	520

Table 14: SVM grid search hyperparameters (ablation study only).

Hyperparameters	Settings
kernel	["linear", "rbf"]
C	[0.1, 1, 10, 100]
gamma (only rbf)	["scale", "auto", 0.001, 0.005, 0.01, 0.05, 0.1, 0.5]
tol	[1e-4, 1e-3]
class weight	[None, "balanced"]

Hyperparameters of pre-training are reported in Table 13, while Table 14 presents the parameters we used in SVM grid search discussed in Appendix B. For complete details of the settings used on downstream datasets, please refer to Appendix E.2. During fine-tuning, we conducted a grid search over the hyperparameters within the ranges specified in Table 15. Owing to the inherent variability and heterogeneity of EEG datasets, we observed that, for certain datasets, reinitializing model weights was essential for NEURIPT to effectively adapt and fine-tune to downstream tasks (i.e., SEED-V, and BCIC-IV-2A). This behavior is likely attributed to a representational mismatch between the pretrained model's and the target task. To address this issue, we performed reinitialization when validation performance showed early saturation during fine-tuning. By resetting the model parameters, this enables the network to escape suboptimal representational basins. Benefiting from distributed data parallelism and FlashAttention-2 [50], the entire pre-training procedure was completed within 30 hours. The subsequent fine-tuning on downstream tasks typically required only a few minutes to several hours, depending on the scale of the specific datasets involved.

Table 15: Hyperparameter tuning ranges used for diverse BCI tasks.

Hyperparameters	Settings
Dropout	0 ~ 0.5
Effective batch size	[4, 8, 16, 32, 64]
Train Epochs	10 ~ 150
Maximum learning rate	$10^{-6} \sim 10^{-4}$
Div factor	1 ~ 5
Final div factor	1 ~ 1e5
Warm up ratio	0 ~ 0.3
Class layers	1 ~ 6
Merge layers	[[1 2 1 2 1 2], [1 4 1 2 1 2], [1 1 8 1 2 1]]
Encoder expert	[[0 0 0 0 0 0], [0 0 2 4 4 6]]
Auxiliary loss weight	0.8 ~ 1
Noise std	0.001 ~ 0.1
W importance	0.001 ~ 0.1
BCE K	0 ~ 0.3
Freeze epochs	0 ~ 50

Table 16: The number of parameters in different methods.

Methods	Activated Params.
EEGNet [52]	0.003M
EEGConformer [53]	0.55M
SPaRCNet [54]	0.79M
ContraWR [23]	1.6M
CNN-Transformer [55]	3.2M
FFCL [6]	2.4M
ST-Transformer [8]	3.5M
BIOT [NeurIPS23] [17]	3.2M
LaBraM-Base [ICLR24] [18]	5.8M
LaBraM-Huge [ICLR24] [18]	369.0M
EEGPT [NeurIPS24] [20]	25.0M
CBraMod [ICLR25] [21]	4.2M
NeuroLM-XL [ICLR25] [19]	1696.0M
NEURIPT (Ours)	73.5M

D.2 Baselines and Metrics

Baselines We compare NEURIPT against eight non-foundation methods— BENDR [15], EEGNet [52], EEGConformer [53], SPaRCNet [54], ContraWR [23], CNN-Transformer [55], FFCL [6], and ST-Transformer [8] —and five foundational model baselines: BIOT [17], LaBraM [18], EEGPT [20], NeuroLM [19], and CBraMod [21]. For any model without published downstream results, we directly followed the results reported in CBraMod [21] and EEGPT [20]. Strictly following the settings of CBraMod, we fine-tune BIOT and LaBraM based on their open-source code and pre-trained weights, unless their experimental results have already been reported in the original papers. Table 16 demonstrates the number of activated parameters for different baselines.

Metrics For binary classification tasks, we report Balanced Accuracy, Area Under the Precision–Recall Curve (AUC-PR), and Area Under the ROC curve (AUROC). For multi-class tasks, we use Balanced Accuracy, Cohen's Kappa, and Weighted F1 score. Note that for PhysioP300, we replace AUC-PR with Cohen's Kappa to match the evaluation protocol of our EEGPT baseline [20]. More details about the metrics we used:

- **Balanced Accuracy**: the average recall across all classes, mitigating class imbalance;
- **AUC-PR**: the area under the precision-recall curve;
- **AUROC**: the area under the receiver operating characteristic curve;
- **Cohen's Kappa**: a measure of inter-rater agreement that accounts for chance, computed based on observed versus expected agreement in a confusion matrix;
- **Weighted F1 Score**: the harmonic mean of precision and recall, weighted by class frequency.

E Dataset Description

E.1 Pre-training Datasets

Table 17 presents the statistics of the datasets used for pre-training NEURIPT.

Table 17: Overview of pretraining datasets.

Datasets	Subject	Total Time
Emobrain	16	4.94h
Grasp and Lift EEG challenge	12	11.72h
Inria BCI Challenge	26	29.98h
EEG Motor Movement/Imagery	109	47.30h
Raw EEG Data	58	34.35h
Resting State EEG Date	22	3.04h
SEED-Series	46	166.75h
Siena Scalp EEG Database	14	30.47h
SPIS Resting State Dataset	10	0.83h
Target Versus Non-Target	50	16.00h
TUAR	213	92.22h
TUEP	200	591.22h
TUSZ	315	1,138.53h
TUSL	38	20.59h

E.1.1 Description of Pre-training Datasets

Emobrain [56] A multimodal emotion dataset contains fNIRS and 64-channel EEG recordings at a sampling rate of 1024 Hz. EEGs are recorded by the Biosemi Active 2 acquisition system, including 16 subjects.Emotional responses were induced using a subset of the IAPS dataset.

Grasp and Lift EEG challenge [57] A dataset containing 32-channel EEG recordings at a sampling rate of 500 Hz. It includes data from 12 subjects performing grasp-and-lift (GAL) trials. EEG signals were recorded using an EEG cap in conjunction with a BrainAmp EEG signal amplifier.

Inria BCI Challenge [58] A P300-Speller dataset that includes 26 subjects with 56-channel EEG recordings at a sampling rate of 600 Hz using Ag/AgCl EEG sensors (VSM-CTF compatible system).

EEG Motor Movement/Imagery [59] A motor imagery dataset comprises EEG recordings from 109 subject performing 2 baseline tasks (eyes-open and eyes-closed), motor movement and motor imagery (both fists or both feet).The EEGs were collected using 64 channels at a sampling rate of 160 Hz with the BCI2000 system.

Raw EEG Data [60] A dataset containing 64-channel EEG recordings sampled at 256 Hz, recorded during the reported Information-Integration categorization task and the reported multidimensional Rule-Based categorization task.

Resting State EEG Date [61] An EEG dataset (64 channels, 256 Hz) containing 22 subjects for a resting task of 8 mins with 4 mins of eyes closed and 4 mins of eyes open using active Ag/AgCl electrodes either mounted in a BioSemi electrode cap or via freestanding electrodes.

SEED-Series [62, 63, 64] A series of datasets, including SEED, SEED-IV, SEED-GER, SEED-FRA. All EEG signals were recorded from 62 channels at a sampling rate of 1000 Hz with the ESI NeuroScan System in response to videos.

Siena Scalp EEG Database [65] A database consists of 31-channel EEG recordings from 14 patients, collected at a sampling rate of 512 Hz using EB Neuro and Natus Quantum LTM amplifiers, along with reusable silver/gold cup electrodes.

SPIS Resting State Dataset [66] A dataset including recordings from 10 subjects, with 2.5-minute EEG segments collected in both eyes-closed and eyes-open resting states, prior to a 105-minute session of Sustained Attention to Response Task (SART) using fixed-sequence and varying ISIs. Monopolar EEG activity (64 channels, 2048 Hz) was recorded using 64 Ag/AgCl active electrodes.

Target Versus Non-Target [67] A P300 dataset including 32-channel EEG signals at a sampling rate of 512 Hz from 50 subjects.

TUAR [68] This subset of TUEG contains EEG recordings annotated with 5 different artifacts, recorded from 23 channels at a sampling rate of 256 Hz.

TUEP [69] This subset of the TUEG comprising EEG recordings from 100 subjects with epilepsy and 100 subjects without epilepsy, as determined by a certified neurologist. The EEG was recorded using 19-23 channels at a sampling rate of 256 Hz.

TUSZ [70] This corpus contains EEG signals that have been manually annotated for seizure events (including start time, stop time, channel, and seizure type). The EEG was recorded using 19-23 channels at a sampling rate of 256 Hz.

TUSL [71] This is another subset of the TUEG containing annotations of slowing events, recorded from 23 channels at 256 Hz. This corpus has been used to study common error modalities in automated seizure detection.

E.1.2 Preprocessing of Pre-training Datasets

In preprocessing, a 0.1–30 Hz band-pass filter was applied to suppress low- and high-frequency noise, followed by a notch filter to eliminate powerline interference. Data were resampled to 64 Hz and segmented into non-overlapping 4-second windows.

To further improve data quality, we removed samples with any signal exceeding 100 μV in absolute amplitude, or with values consistently below 3 μV or above 3 μV across all time points in any channel, as these likely reflect artifacts or flatlining. Subsequently, data were normalized using A-law companding (from digital signal processing) with $A = 0.25$ was used to adjust the dynamic range all EEG signals to ensure consistent scaling. After pre-processing, we retained 2,219,455 EEG segments, totaling over 2,100 hours of clean data for pre-training.

E.2 Downstream Datasets

E.2.1 Description of Downstream Datasets

I. Mental Stress Detection This task focuses on identifying an individual's stress level using EEG signals. The MentalArithmetic dataset [72, 73] contains EEG recordings from 36 subjects of varying genders and ages, collected both before and during the performance of mental arithmetic tasks.

II. Mental Disorder Diagnosis This task aims to categorize mental health states based on EEG activity. The Mumtaz2016 dataset [74] comprises EEG recordings from 34 patients diagnosed with major depressive disorder and 30 healthy control subjects.

III. P300 Task This task involves detecting the P300 wave, an event-related potential reflecting cognitive processes such as attention, stimulus evaluation, and target recognition. The PhysioNetP300 dataset [75] provides EEG recordings commonly used for benchmarking P300-based brain–computer interface studies.

IV. Sleep Staging Detection This task aims to classify sleep stages based on polysomnographic EEG recordings. The SleepEDFx dataset [76] contains 197 whole-night recordings and is widely used as a benchmark for automated sleep staging.

V. Emotion Recognition This task concerns the detection and interpretation of emotional states from EEG data. The SEED-V dataset [3] provides EEG recordings collected while subjects watched emotionally evocative videos.

VI. Motor Imagery Task This task focuses on decoding motor imagery activities from EEG signals. The BCI Competition IV-2A dataset [4] consists of EEG recordings from 9 healthy subjects performing four types of motor imagery tasks.

VII. Abnormal Detection This task involves identifying abnormal neural patterns in EEG data. We followed CBraMod [21], TUAB [2] was chosen as the downstream dataset for this task. The TUAB dataset [2], a large-scale clinical EEG corpus, provides recordings annotated for abnormal events and has been widely used for automated abnormality detection.

VIII. Event Type Classification This task focuses on categorizing EEG segments into distinct event types. Similarly, following CBraMod [21], TUEV [2] was chosen as the downstream dataset for this task. The TUEV dataset [2] includes EEG recordings annotated for epileptic and non-epileptic events, making it a standard resource for event-type classification studies.

E.2.2 Mental Stress Detection: MentalArithmetic (2-class)

MentalArithmetic [72, 73] is an EEG dataset that contains recordings of 36 subjects of different genders and ages before and during the performance of mental arithmetic tasks. The EEGs are recorded from 20 silver/silver chloride electrodes placed according to the international 10-20 system at 500Hz sampling rate. All EEG recordings during mental arithmetic are labeled "under stress". The ones that are not during mental arithmetic are labeled "no stress". We present the analysis of expert participation on this dataset in Figure 10.The channel relationships are visualized in Figure 8.

Table 18: Comparison of different methods on mental stress detection (MentalArithmetic, 2-class).

Method	Balanced Accuracy	AUC-PR	AUROC
EEGNet [52]	0.6770 ± 0.0116	0.5763 ± 0.0102	0.7321 ± 0.0108
EEGConformer [53]	0.6805 ± 0.0123	0.5829 ± 0.0134	0.7424 ± 0.0128
SPaRCNet [54]	0.6879 ± 0.0107	0.5825 ± 0.0193	0.7418 ± 0.0132
ContraWR [23]	0.6631 ± 0.0097	0.5787 ± 0.0164	0.7332 ± 0.0082
CNN-Transformer [55]	0.6779 ± 0.0268	0.5777 ± 0.0285	0.7258 ± 0.0336
FFCL [6]	0.6798 ± 0.0142	0.5786 ± 0.0266	0.7330 ± 0.0198
ST-Transformer [8]	0.6631 ± 0.0173	0.5672 ± 0.0259	0.7132 ± 0.0174
BIOT [NeurIPS23] [17]	0.6875 ± 0.0186	0.6004 ± 0.0195	0.7536 ± 0.0144
LaBraM [ICLR24] [18]	0.6909 ± 0.0125	0.5999 ± 0.0155	0.7721 ± 0.0093
CBraMod [ICLR25] [21]	0.7256 ± 0.0132	0.6267 ± 0.0099	0.7905 ± 0.0073
NEURIPT (Ours)	**0.8646** ± 0.0107	**0.7827** ± 0.0197	**0.9111** ± 0.0163

Preprocessing All data were first converted to uniform units. A 50 Hz notch filter was applied to attenuate power-line noise, followed by resampling the data to 64 Hz. A global average reference was then used. And following CBraMod [21], the data were segmented into 5-seconds.

Experimental Configuration Following CBraMod [21], subject 1 to 28 are set to training set, subject 29 to 32 are set to validation set and subject 33 to 36 are set to test set.

Results As shown in Table 18, NEURIPT achieves the state-of-the-art performance and gets a great improvement. NEURIPT performs 13.9 % better than the best baseline in balanced accurary, 15.6 % better than the best baseline in AUC-PR and 12.06 % better than the best baseline in AUROC.

E.2.3 Mental Disorder Diagnosis: Mumtaz2016 (2-class)

Mumtaz2016 [74] consists of EEG recordings from 34 patients diagnosed with major depressive disorder (MDD) and 30 healthy subjects (H). All EEGs recorded from 19 electrodes placed according to the international 10–20 system at 256Hz sampling rate. The dataset collects three sessions, including eyes-open session, eyes-closed session, and task session. We present the analysis of expert participation on this dataset in Figure 11. The channel relationships are visualized in Figure 8.

Preprocessing The data were first converted to uniform units. A 50 Hz notch filter was then applied to attenuate power-line noise. After that, the data were resampled to 64 Hz and re-referenced using a global average reference. Following CBraMod [21], the data were segmented into 5-seconds.

Experimental Configuration In our experiment, we only uses eyes-open session and eyes-closed session. Similarly, following CBraMod [21], 24 MDD and 19 H are used for training,5 MDD and 4 H are used for validation, and 5 MDD and 5 H are used for test.

Table 19: Comparison of different methods on mental disorder diagnosis (Mumtaz2016, 2-class).

Method	Balanced Accuracy	AUC-PR	AUROC
EEGNet [52]	0.9232 ± 0.0104	0.9626 ± 0.0095	0.9639 ± 0.0093
EEGConformer [53]	0.9308 ± 0.0117	0.9684 ± 0.0105	0.9702 ± 0.0101
SPaRCNet [54]	0.9316 ± 0.0095	0.9754 ± 0.0065	0.9781 ± 0.0083
ContraWR [23]	0.9195 ± 0.0115	0.9589 ± 0.0102	0.9621 ± 0.0092
CNN-Transformer [55]	0.9305 ± 0.0068	0.9757 ± 0.0074	0.9742 ± 0.0059
FFCL [6]	0.9314 ± 0.0038	0.9717 ± 0.0021	0.9753 ± 0.0033
ST-Transformer [8]	0.9135 ± 0.0103	0.9578 ± 0.0086	0.9594 ± 0.0059
BIOT [NeurIPS23] [17]	0.9358 ± 0.0052	0.9736 ± 0.0034	0.9758 ± 0.0042
LaBraM [ICLR24] [18]	0.9409 ± 0.0079	0.9798 ± 0.0093	0.9782 ± 0.0057
CBraMod [ICLR25] [21]	0.9560 ± 0.0056	0.9923 ± 0.0032	0.9921 ± 0.0025
NEURIPT (Ours)	**0.9803** ± 0.0062	**0.9981** ± 0.0044	**0.9979** ± 0.0045

Results As shown in Table 19, NEURIPT achieves the state-of-the-art performance. NEURIPT performs 2.43 % better than the best baseline in balanced accuracy.

E.2.4 P300 Task: PhysioNetP300 (2-class)

PhysioNetP300 [75] is typical P300 task dataset. Each record in the dataset contains the signals, triggers and annotations corresponding to a single run. In this dataset, each subject was asked to spell a total of 20 characters using a Donchin speller. The target characters were randomly selected before the start of the run. Each row and column of a standard 6x6 character matrix was randomly augmented for 100 ms at 50 ms intervals with approximately 20 flashes. During this time, subjects need to focus on the target and count the number of times the target was highlighted. When the target was highlighted, we labeled it as "Target". Otherwise, we label it as "Non-target". We present the analysis of expert participation on this dataset in Figure 12. The channel relationships are visualized in Figure 8.

Table 20: The results of different methods on P300 task (PhysioNetP300, 2-class).

Methods	Balanced Accuracy	Cohen's Kappa	AUROC
BENDR [15]	0.6114 ± 0.0118	0.2227 ± 0.0237	0.6588 ± 0.0163
BIOT [NeurIPS23] [17]	0.5485 ± 0.0325	0.0968 ± 0.0647	0.5308 ± 0.0333
LaBraM [ICLR24] [18]	0.6477 ± 0.0110	0.2935 ± 0.0227	0.7068 ± 0.0134
EEGPT [NeurIPS24] [20]	0.6502 ± 0.0063	0.2999 ± 0.0139	0.7168 ± 0.0051
NEURIPT (Ours)	**0.6731** ± 0.0045	**0.3426** ± 0.0074	**0.7683** ± 0.0039

Preprocessing The data were first converted to uniform units. A 60 Hz notch filter was applied to attenuate power-line noise. The signals were then resampled to 64 Hz and re-referenced using a global average reference. Following the preprocessing steps used in EEGPT [20], the data were segmented into 2-seconds starting at 0.7 seconds before the onset of the flicker stimulus.

Experimental Configuration Following EEGPT [20], subjects 8, 10, and 12 were removed and the data from the remaining subjects were retained. We split the subjects into training set and testing set randomly.

Results As shown in Table 20, NEURIPT achieves the state-of-the-art performance. NEURIPT performs better than the best baseline in all 3 evaluation metrics.

E.2.5 Sleep Stage Detection: SleepEDFx (5-class)

SleepEDFx [76] is a dataset that contains 197 (78 healthy subjects) whole-night polysomnographic sleep recordings, including EEG, EOG, chin EMG, and event markers. The sampling rate are 100Hz of the EEG and EOG channels, the ohter channels are 1Hz. We present the analysis of expert participation on this dataset in Figure 13. The channel relationships are visualized in Figure 8.

Table 21: The results of different methods on sleep stage detection (SleepEDFx, 5-class).

Methods	Balanced Accuracy	Cohen's Kappa	Weighted F1
BENDR [15]	0.6655 ± 0.0043	0.6659 ± 0.0043	0.7507 ± 0.0029
BIOT [NeurIPS23] [17]	0.6622 ± 0.0013	0.6461 ± 0.0017	0.7415 ± 0.0010
LaBraM [ICLR24] [18]	0.6771 ± 0.0022	0.6710 ± 0.0006	0.7592 ± 0.0005
EEGPT [NeurIPS24] [20]	0.6917 ± 0.0069	0.6857 ± 0.0019	0.7654 ± 0.0023
NEURIPT (Ours)	**0.7047** ± 0.0041	**0.7757** ± 0.0015	**0.8739** ± 0.0013

Preprocessing The data were first converted to uniform units. They were then resampled to 64 Hz and re-referenced using a global average reference. Following EEGPT [20], the data were segmented into 30-seconds.

Experimental Configuration We use the whole sleep-cassette (SC) and sleep-telemetry (ST) dataset that includes 197 subjects. Following EEGPT [20], subjects were randomly divided according to the ratio of 60.

Results As shown in Table 21, NEURIPT achieves the state-of-the-art performance. NEURIPT performs better than the best baseline in all 3 evaluation metrics. In particular, NEURIPT gets a great improvement in Cohen's Kappa and Weighted F1.

E.2.6 Emotion Recognition: SEED-V (4-class)

The SEED-V dataset [3] comprises EEG and eye movement recordings from 16 participants during emotion elicitation tasks. Each participant completed three sessions on separate days, with each session containing 15 trials—three trials for each of five emotion categories: happy, sad, neutral, disgust, and fear. EEG signals were recorded using a 62-channel ESI NeuroScan system at a sampling rate of 1000 Hz. The dataset provides both raw EEG data and extracted differential entropy (DE) features across five frequency bands, facilitating various analyses in emotion recognition research. We also present the analysis of expert participation on the this dataset in Figure 14, and report the Pearson correlation between class logits and channel perturbations induced by Gaussian multiplicative noise in Figure 16. The channel relationships are visualized in Figure 8.

Table 22: The results of different methods on emotion recognition (SEED-V, 5-class).

Methods	Balanced Accuracy	Cohen's Kappa	Weighted F1
EEGNet [52]	0.2961 ± 0.0102	0.1006 ± 0.0143	0.2749 ± 0.0098
EEGConformer [53]	0.3537 ± 0.0112	0.1772 ± 0.0174	0.3487 ± 0.0136
SPaRCNet [54]	0.2949 ± 0.0078	0.1121 ± 0.0139	0.2979 ± 0.0083
ContraWR [23]	0.3546 ± 0.0105	0.1905 ± 0.0188	0.3544 ± 0.0121
CNN-Transformer [55]	0.3678 ± 0.0078	0.2072 ± 0.0183	0.3642 ± 0.0088
FFCL [6]	0.3641 ± 0.0092	0.2078 ± 0.0201	0.3645 ± 0.0132
ST-Transformer [8]	0.3052 ± 0.0072	0.1083 ± 0.0121	0.2833 ± 0.0105
BIOT [NeurIPS23] [17]	0.3837 ± 0.0187	0.2261 ± 0.0262	0.3856 ± 0.0203
LaBraM [ICLR24] [18]	0.3976 ± 0.0138	0.2386 ± 0.0209	0.3974 ± 0.0111
CBraMod [ICLR25] [21]	0.4091 ± 0.0097	0.2569 ± 0.0143	0.4101 ± 0.0108
NEURIPT (Ours)	**0.4104** ± 0.0021	**0.2629** ± 0.0039	**0.4158** ± 0.0037

Preprocessing EEG signals were band-pass filtered between 0.1 Hz and 30 Hz and downsampled to 64 Hz. A 50 Hz notch filter was applied to remove power line interference. Each trial was segmented into non-overlapping 1-second epochs, resulting in a total of 115,001 samples. Following CBraMod [21], data from subjects 1–10 were used for training, while subjects 11–15 were reserved for testing. Detailed results are reported in Table 22.

Experimental Configuration Each 1-second segment was treated as an independent sample labeled according to the corresponding emotion category. The model was trained for 10 epochs using a batch size of 256. We use both bipolar and non-bipolar methods, and the non-bipolar one is slightly better than the bipolar one.

Results Our proposed NEURIPT model achieves state-of-the-art performance on SEED-V emotion recognition task, outperforming existing models across the evaluation metrics. These results highlight the effectiveness and robustness of our approach in modeling complex emotional dynamics from EEG signals.

E.2.7 Motor Imagery Task: BCIC-IV-2A (4-class)

The BCIC-IV-2A dataset [4] comprises EEG recordings from 9 healthy subjects performing 4 motor-imagery tasks: left hand (Class 1), right hand (Class 2), feet (Class 3) and tongue (Class 4). Each subject completed two sessions on separate days; each session contains six runs of 48 trials (12 trials per class), yielding 288 trials per session. Signals were acquired at 250 Hz from 22 channels positioned according to the international 10–20 system and band-pass filtered between 0.5 Hz and 100 Hz. We also present the analysis of expert participation on the this dataset in Figure 6, and report the Pearson correlation between class logits and channel perturbations induced by Gaussian multiplicative noise in Figure 4. The channel relationships are visualized in Figure 8.

Table 23: The results of different methods on motor imagery classification (BCIC-IV-2A, 4-class).

Methods	Balanced Accuracy	Cohen's Kappa	Weight F1
EEGNet [52]	0.4482 ± 0.0094	0.2693 ± 0.0121	0.4226 ± 0.0108
EEGConformer [53]	0.4696 ± 0.0106	0.2924 ± 0.0141	0.4533 ± 0.0128
SPaRCNet [54]	0.4635 ± 0.0117	0.2847 ± 0.0147	0.4432 ± 0.0126
ContraWR [23]	0.4678 ± 0.0125	0.2905 ± 0.0160	0.4413 ± 0.0142
CNN-Transformer [55]	0.4600 ± 0.0108	0.2800 ± 0.0148	0.4460 ± 0.0114
FFCL [6]	0.4470 ± 0.0143	0.2627 ± 0.0176	0.4238 ± 0.0139
ST-Transformer [8]	0.4575 ± 0.0145	0.2733 ± 0.0198	0.4471 ± 0.0142
BIOT [NeurIPS23] [17]	0.4748 ± 0.0093	0.2997 ± 0.0139	0.4607 ± 0.0125
LaBraM [ICLR24] [18]	0.4869 ± 0.0085	0.3159 ± 0.0154	0.4758 ± 0.0103
CBraMod [ICLR25] [21]	0.5138 ± 0.0066	0.3518 ± 0.0094	0.4984 ± 0.0085
NEURIPT (Ours)	**0.5504** ± 0.0072	**0.4005** ± 0.0121	**0.5376** ± 0.0086

Preprocessing Raw EEG signals were band-pass filtered between 0.1 Hz and 30 Hz, followed by downsampling to 64 Hz. For each trial, we extracted the segment from 2 s to 6 s after cue onset and assigned labels according to the instructed motor imagery class. This procedure yielded 288 non-overlapping 4 s segments per session. Signals were re-referenced using 16 predefined bipolar channel pairs. The model input comprised the 16 bipolar channels. Following CBraMod [21], data from subjects 1–5 were used for training, subjects 6–7 for validation, and subjects 8–9 for testing. The detailed channel configuration and corresponding sample counts are provided in Table 23.

Experimental Configuration Optimization employed a cosine-annealed learning rate schedule, warming up linearly from 1.7×10^{-5} to 3.5×10^{-5}, then decaying back to 1.7×10^{-5} by epoch 150. We trained with a batch size of 16 for 150 epochs.

Results Our proposed NEURIPT model achieves state-of-the-art performance on BCIC-IV-2A motor imagery classification, outperforming existing baselines across all evaluation metrics. These results demonstrate the effectiveness and robustness of our approach.

E.2.8 Abnormal Detection: TUAB (2-class) and Event Type Classification: TUEV (6-class)

The TUEV dataset [2] is a curated subset of the Temple University Hospital EEG Corpus (TUEG), enriched with expert annotations for epileptiform and non-epileptiform events. Each EEG segment is labeled into one of six categories: spikes and sharp waves (Class 1), generalized periodic epileptiform discharges (Class 2), periodic unilateral epileptiform discharges (Class 3), eye movements (Class 4), artifacts (Class 5), and background (Class 6). Recordings were acquired using 23 EEG channels with a sampling rate of 250 Hz. We present the analysis of expert participation on this dataset in Figure 15. The channel relationships are visualized in Figure 8.

The TUAB dataset [2] is a large-scale EEG corpus annotated for abnormality detection. Each recording is labeled as either normal or abnormal based on clinical reports. Similar to TUEV, the EEG signals were recorded using 23 channels with a sampling rate of 250 Hz. The dataset serves as a benchmark for evaluating automated EEG abnormality detection methods. We present the analysis of expert participation on this dataset in Figure 9. The channel relationships are visualized in Figure 8.

Table 24: Comparison of different methods on TUAB (2-class) and TUEV (6-class).

Method	TUAB			TUEV		
	Balanced Acc.	AUC-PR	AUROC	Balanced Acc.	Cohen's Kappa	Weighted F1
EEGNet [52]	0.7642 ± 0.0036	0.8299 ± 0.0043	0.8412 ± 0.0031	0.3876 ± 0.0143	0.3577 ± 0.0155	0.6539 ± 0.0120
EEGConformer [53]	0.7758 ± 0.0049	0.8427 ± 0.0054	0.8445 ± 0.0038	0.4074 ± 0.0164	0.3967 ± 0.0195	0.6983 ± 0.0152
SPaRCNet [54]	0.7896 ± 0.0018	0.8414 ± 0.0018	0.8676 ± 0.0012	0.4161 ± 0.0262	0.4233 ± 0.0181	0.7024 ± 0.0104
ContraWR [23]	0.7746 ± 0.0041	0.8421 ± 0.0104	0.8456 ± 0.0074	0.4384 ± 0.0349	0.3912 ± 0.0237	0.6893 ± 0.0136
CNN-Transformer [55]	0.7777 ± 0.0022	0.8433 ± 0.0039	0.8461 ± 0.0013	0.4087 ± 0.0161	0.3815 ± 0.0134	0.6854 ± 0.0293
FFCL [6]	0.7848 ± 0.0038	0.8448 ± 0.0065	0.8569 ± 0.0051	0.3979 ± 0.0104	0.3732 ± 0.0188	0.6783 ± 0.0120
ST-Transformer [8]	0.7966 ± 0.0023	0.8521 ± 0.0026	0.8707 ± 0.0019	0.3984 ± 0.0228	0.3765 ± 0.0306	0.6823 ± 0.0190
BIOT[NeurIPS23] [17]	0.7959 ± 0.0057	0.8792 ± 0.0023	0.8815 ± 0.0043	0.5281 ± 0.0225	0.5273 ± 0.0249	0.7492 ± 0.0082
LaBraM-Huge[ICLR24] [18]	0.8258 ± 0.0011	0.9204 ± 0.0011	0.9162 ± 0.0016	0.6616 ± 0.0170	0.6745 ± 0.0195	0.8329 ± 0.0086
EEGPT[NeurIPS24] [20]	0.7983 ± 0.0030	-	0.8718 ± 0.8718	0.6232 ± 0.0114	0.6351 ± 0.0134	0.8187 ± 0.0063
NeuroLM-XL[ICLR25] [19]	0.7969 ± 0.0091	0.7219 ± 0.0082	0.7884 ± 0.0194	0.4679 ± 0.0356	0.4570 ± 0.0498	0.7359 ± 0.0219
CBraMod[ICLR25] [21]	0.8289 ± 0.0022	**0.9258** ± 0.0008	**0.9227** ± 0.0011	0.6671 ± 0.0107	0.6772 ± 0.0096	0.8342 ± 0.0064
NEURIPT (Ours)	**0.8293** ± 0.0016	0.9040 ± 0.0022	0.8949 ± 0.0021	**0.6761** ± 0.0133	**0.6970** ± 0.0185	**0.8428** ± 0.0089

Preprocessing All EEG recordings were band-pass filtered between 0.1 Hz and 30 Hz to attenuate low- and high-frequency noise, and a 60 Hz notch filter was applied to remove power-line interference. Signals were then resampled to 64 Hz and segmented into fixed-length epochs: 5 s non-overlapping segments for TUEV, and 10 s segments for TUAB. We maintained the original training/test partitions provided by each dataset to ensure a fair comparison with the three baselines-LaBraM[18], EEGPT [20] and CBraMod[21]. The training subjects were further divided into training and validation subsets in an 80% / 20% ratio.

Experimental Configuration For TUEV, each 5-second segment was treated as an independent sample labeled according to the corresponding category. The model was trained for 20 epochs using a batch size of 16. The learning rate peaked at 1×10^{-5}, and then gradually decayed to a minimum of 1×10^{-7}. For TUAB, each 10-second segment was treated as an independent sample labeled according to the corresponding category. The model was trained for 10 epochs using a batch size of 16. The learning rate peaked at 5×10^{-6}, and then gradually decayed to a minimum of 3×10^{-7}.

Results Our proposed NEURIPT model achieves state-of-the-art performance on the TUEV dataset, consistently outperforming existing baselines across all evaluation metrics. These results highlight the effectiveness and robustness of our method. On the TUAB abnormality detection task, NEURIPT attains higher balanced accuracy compared to prior methods. While the performance on the other two metrics is slightly lower than the best results, it still exceeds most baseline models. This indicates that NEURIPT is both competitive and effective, demonstrating strong generalization ability in learning transferable EEG representations.

F Discussion

F.1 Limitation

While NEURIPT incorporated several important characteristics of EEG signals into its neural architecture to learn more generalizable representations, there remain several open challenges and opportunities for future work. (1) For instance, additional EEG-specific aspects, such as brain connectivity representations, have not yet been fully explored and could enhance decoding performance. (2) Moreover, as with many foundation models, NEURIPT requires a large number of parameters, resulting in increased memory usage and higher computational costs during both training and inference compared to non-foundation models. (3) Our ability to further scale the model and investigate scaling laws was constrained by the limited GPU resources available. (4) Lastly, although NEURIPT achieved SOTA performance on average across multiple datasets, there is still room to improve neural decoding accuracy to fully meet the practical demands of BCI systems for real-world and clinical applications.

F.2 Broader Impacts

This work advances neural decoding for general EEG-based neural interfaces, with potential benefits across a wide range of BCI applications, including clinical diagnosis, emotion recognition, and user intent control. These advancements have broader implications for enhancing human well-being by expanding access to brain–computer interface (BCI) technologies and enabling more diverse real-world applications. While our method is primarily developed for foundation models (FMs), it is designed to leverage key EEG characteristics, making it also adaptable to task- and setup-specific models for a wide range of application-specific scenarios. Furthermore, our findings provide valuable insights for the development of more advanced foundation models that incorporate other EEG-specific characteristics, such as brain connectivity.

F.3 Potential Misuse

As EEG foundation models become increasingly powerful for healthcare and brain–computer interface (BCI) applications, it is crucial to acknowledge their potential for misuse, for example, unauthorized cognitive surveillance or profiling. The ability to infer mental states or cognitive intent, if applied without proper oversight, raises profound ethical concerns. Addressing these risks will require the development of neurotechnology regulations, data protection policies, and ethics frameworks to ensure responsible use and safeguard individual neural privacy.

G Further Visualization

Further visualizations start on the next page.

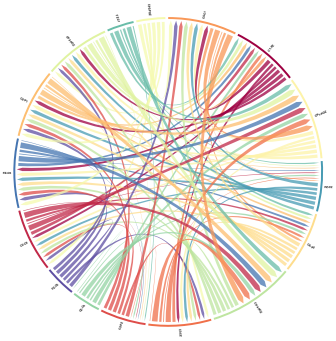

(a) BCIC-IV-2A

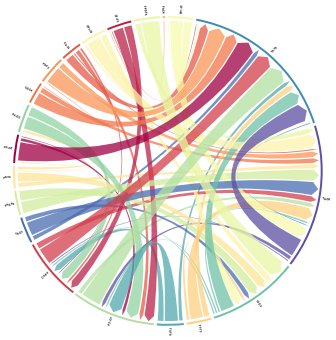

(b) MentalArithmetic

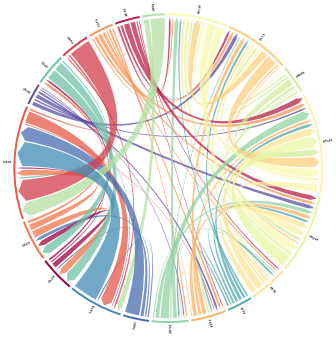

(c) Mumtaz 2016

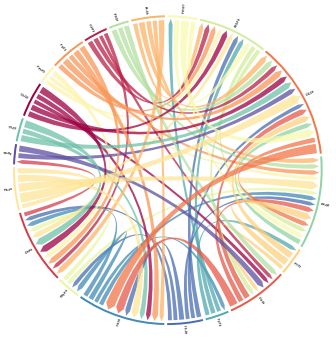

(d) PhysioNetP300

(e) TUEV

(f) TUAB

(g) SEED-V

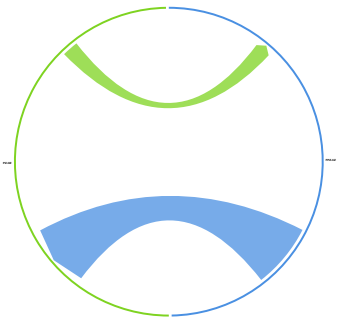

(h) Sleep-EDFx

Figure 8: Inter-channel relationships for eight downstream tasks.

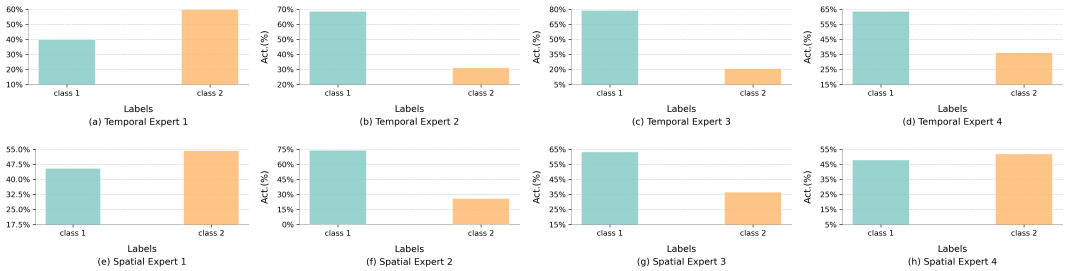

Figure 9: Analysis of expert participation on the TUAB dataset.

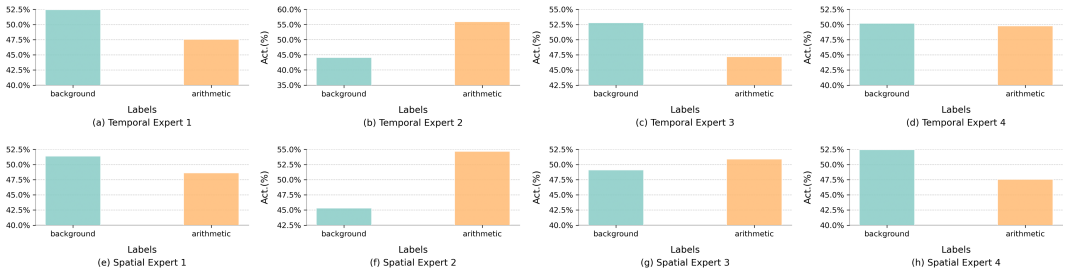

Figure 10: Analysis of expert participation on the MentalArithmetic dataset.

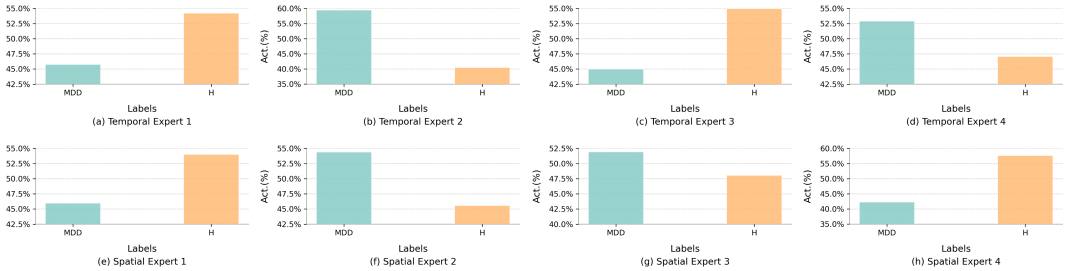

Figure 11: Analysis of expert participation on the Mumtaz dataset.

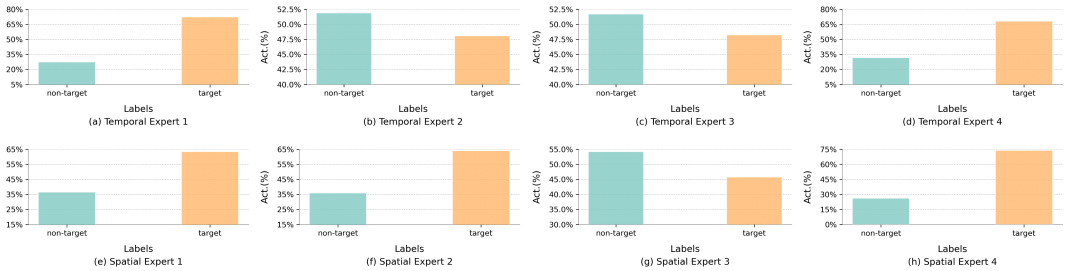

Figure 12: Analysis of expert participation on the P300 dataset.

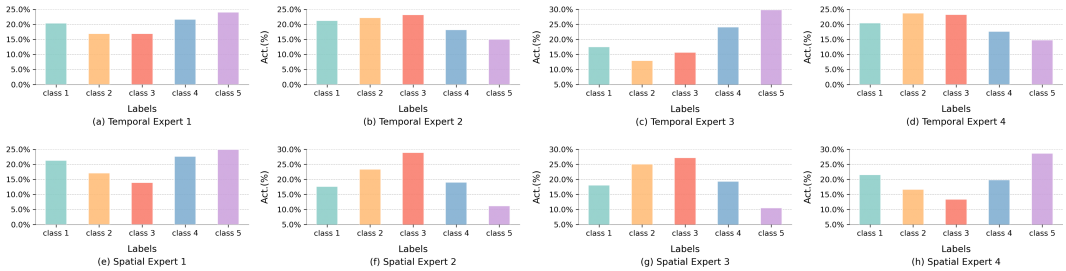

Figure 13: Analysis of expert participation on the SleepEDF dataset.

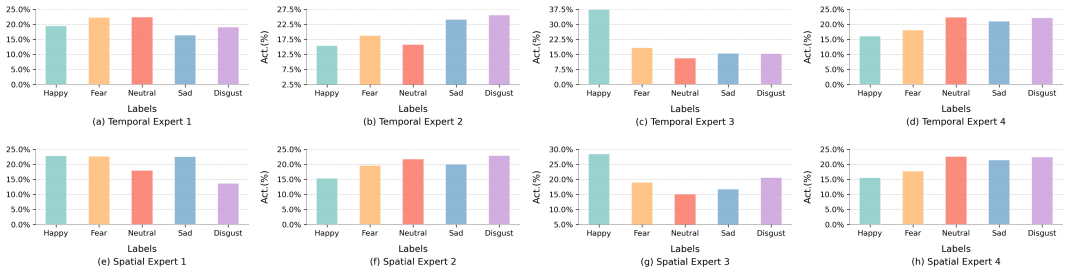

Figure 14: Analysis of expert participation on the SEED-V dataset.

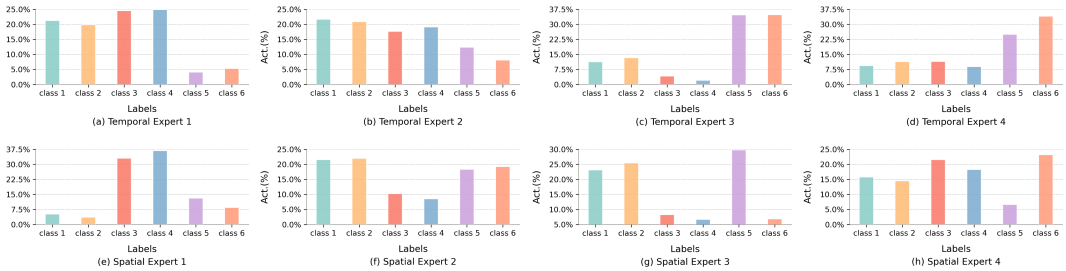

Figure 15: Analysis of expert participation on the TUEV dataset.

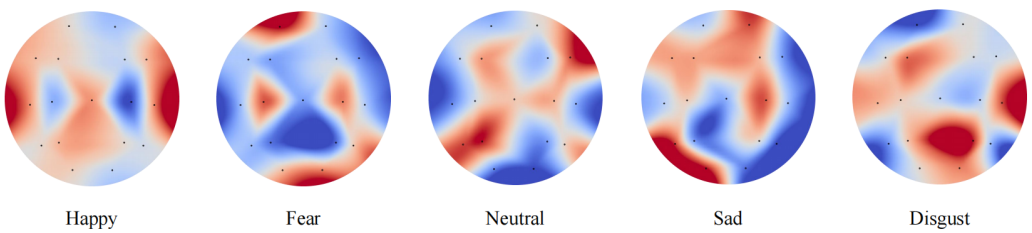

Figure 16: Pearson correlation between class logits and channel perturbation using Gaussian multiplicative noise on SEED-V.

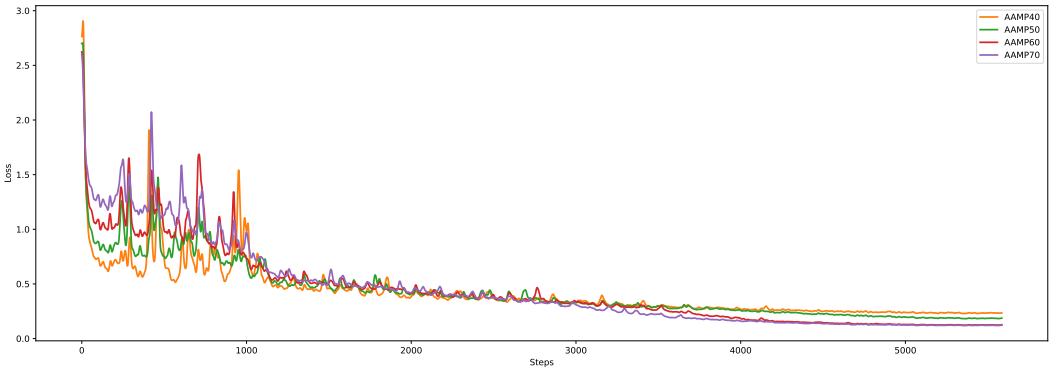

Figure 17: Loss with different mask ratios

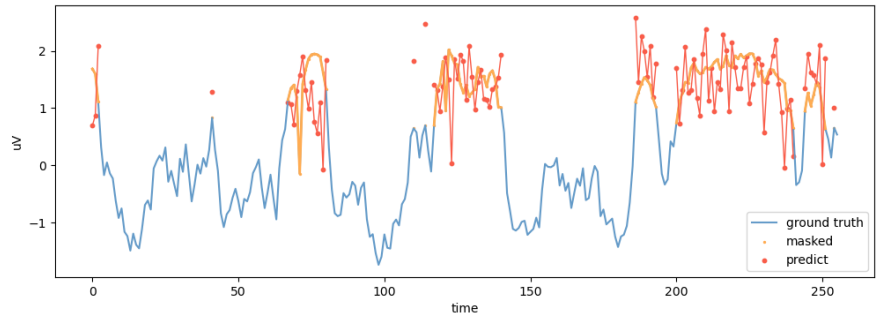

Figure 18: Visualization of AAMP based reconstruction (a).

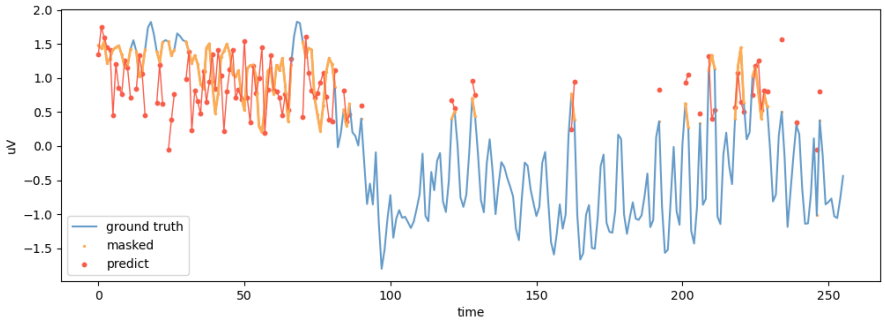

Figure 19: Visualization of AAMP based reconstruction (b).

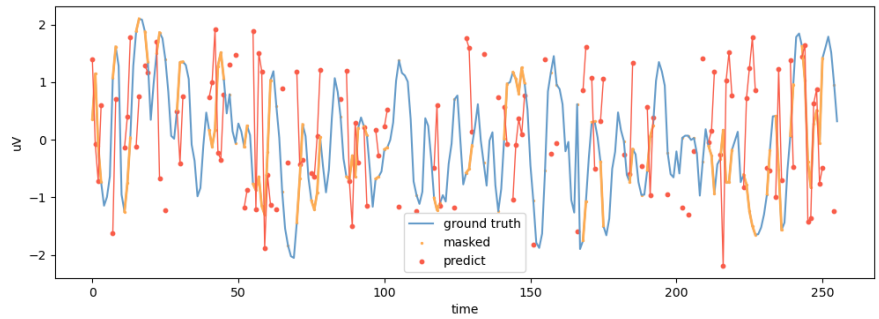

Figure 20: Visualization of reconstruction with BERT-style masking.

NeurIPS Paper Checklist

1. **Claims**

   Question: Do the main claims made in the abstract and introduction accurately reflect the paper's contributions and scope?

   Answer: [Yes]

   Justification: Double checked carefully.

   Guidelines:

   - The answer NA means that the abstract and introduction do not include the claims made in the paper.
   - The abstract and/or introduction should clearly state the claims made, including the contributions made in the paper and important assumptions and limitations. A No or NA answer to this question will not be perceived well by the reviewers.
   - The claims made should match theoretical and experimental results, and reflect how much the results can be expected to generalize to other settings.
   - It is fine to include aspirational goals as motivation as long as it is clear that these goals are not attained by the paper.

2. **Limitations**

   Question: Does the paper discuss the limitations of the work performed by the authors?

   Answer: [Yes]

   Justification: It is provided in the Appendix Section F.1.

   Guidelines:

   - The answer NA means that the paper has no limitation while the answer No means that the paper has limitations, but those are not discussed in the paper.
   - The authors are encouraged to create a separate "Limitations" section in their paper.
   - The paper should point out any strong assumptions and how robust the results are to violations of these assumptions (e.g., independence assumptions, noiseless settings, model well-specification, asymptotic approximations only holding locally). The authors should reflect on how these assumptions might be violated in practice and what the implications would be.
   - The authors should reflect on the scope of the claims made, e.g., if the approach was only tested on a few datasets or with a few runs. In general, empirical results often depend on implicit assumptions, which should be articulated.
   - The authors should reflect on the factors that influence the performance of the approach. For example, a facial recognition algorithm may perform poorly when image resolution is low or images are taken in low lighting. Or a speech-to-text system might not be used reliably to provide closed captions for online lectures because it fails to handle technical jargon.
   - The authors should discuss the computational efficiency of the proposed algorithms and how they scale with dataset size.
   - If applicable, the authors should discuss possible limitations of their approach to address problems of privacy and fairness.
   - While the authors might fear that complete honesty about limitations might be used by reviewers as grounds for rejection, a worse outcome might be that reviewers discover limitations that aren't acknowledged in the paper. The authors should use their best judgment and recognize that individual actions in favor of transparency play an important role in developing norms that preserve the integrity of the community. Reviewers will be specifically instructed to not penalize honesty concerning limitations.

3. **Theory assumptions and proofs**

   Question: For each theoretical result, does the paper provide the full set of assumptions and a complete (and correct) proof?

   Answer: [NA]

Justification: This work does not make theoretical assumptions.

Guidelines:

- The answer NA means that the paper does not include theoretical results.
- All the theorems, formulas, and proofs in the paper should be numbered and cross-referenced.
- All assumptions should be clearly stated or referenced in the statement of any theorems.
- The proofs can either appear in the main paper or the supplemental material, but if they appear in the supplemental material, the authors are encouraged to provide a short proof sketch to provide intuition.
- Inversely, any informal proof provided in the core of the paper should be complemented by formal proofs provided in appendix or supplemental material.
- Theorems and Lemmas that the proof relies upon should be properly referenced.

4. **Experimental result reproducibility**

   Question: Does the paper fully disclose all the information needed to reproduce the main experimental results of the paper to the extent that it affects the main claims and/or conclusions of the paper (regardless of whether the code and data are provided or not)?

   Answer: [Yes]

   Justification: The information is detailed in Section 3 and Appendix D with source code provided.

   Guidelines:

   - The answer NA means that the paper does not include experiments.
   - If the paper includes experiments, a No answer to this question will not be perceived well by the reviewers: Making the paper reproducible is important, regardless of whether the code and data are provided or not.
   - If the contribution is a dataset and/or model, the authors should describe the steps taken to make their results reproducible or verifiable.
   - Depending on the contribution, reproducibility can be accomplished in various ways. For example, if the contribution is a novel architecture, describing the architecture fully might suffice, or if the contribution is a specific model and empirical evaluation, it may be necessary to either make it possible for others to replicate the model with the same dataset, or provide access to the model. In general. releasing code and data is often one good way to accomplish this, but reproducibility can also be provided via detailed instructions for how to replicate the results, access to a hosted model (e.g., in the case of a large language model), releasing of a model checkpoint, or other means that are appropriate to the research performed.
   - While NeurIPS does not require releasing code, the conference does require all submissions to provide some reasonable avenue for reproducibility, which may depend on the nature of the contribution. For example
     (a) If the contribution is primarily a new algorithm, the paper should make it clear how to reproduce that algorithm.
     (b) If the contribution is primarily a new model architecture, the paper should describe the architecture clearly and fully.
     (c) If the contribution is a new model (e.g., a large language model), then there should either be a way to access this model for reproducing the results or a way to reproduce the model (e.g., with an open-source dataset or instructions for how to construct the dataset).
     (d) We recognize that reproducibility may be tricky in some cases, in which case authors are welcome to describe the particular way they provide for reproducibility. In the case of closed-source models, it may be that access to the model is limited in some way (e.g., to registered users), but it should be possible for other researchers to have some path to reproducing or verifying the results.

5. **Open access to data and code**

   Question: Does the paper provide open access to the data and code, with sufficient instructions to faithfully reproduce the main experimental results, as described in supplemental material?

Answer: [Yes]

Justification: We provide our project link in the Abstract, which includes the source code and instructions.

Guidelines:

- The answer NA means that paper does not include experiments requiring code.
- Please see the NeurIPS code and data submission guidelines (https://nips.cc/public/guides/CodeSubmissionPolicy) for more details.
- While we encourage the release of code and data, we understand that this might not be possible, so "No" is an acceptable answer. Papers cannot be rejected simply for not including code, unless this is central to the contribution (e.g., for a new open-source benchmark).
- The instructions should contain the exact command and environment needed to run to reproduce the results. See the NeurIPS code and data submission guidelines (https://nips.cc/public/guides/CodeSubmissionPolicy) for more details.
- The authors should provide instructions on data access and preparation, including how to access the raw data, preprocessed data, intermediate data, and generated data, etc.
- The authors should provide scripts to reproduce all experimental results for the new proposed method and baselines. If only a subset of experiments are reproducible, they should state which ones are omitted from the script and why.
- At submission time, to preserve anonymity, the authors should release anonymized versions (if applicable).
- Providing as much information as possible in supplemental material (appended to the paper) is recommended, but including URLs to data and code is permitted.

6. **Experimental setting/details**

   Question: Does the paper specify all the training and test details (e.g., data splits, hyperparameters, how they were chosen, type of optimizer, etc.) necessary to understand the results?

   Answer: [Yes]

   Justification: It is detailed in Section 3.

   Guidelines:

   - The answer NA means that the paper does not include experiments.
   - The experimental setting should be presented in the core of the paper to a level of detail that is necessary to appreciate the results and make sense of them.
   - The full details can be provided either with the code, in appendix, or as supplemental material.

7. **Experiment statistical significance**

   Question: Does the paper report error bars suitably and correctly defined or other appropriate information about the statistical significance of the experiments?

   Answer: [Yes]

   Justification: The numerical results are provided.

   Guidelines:

   - The answer NA means that the paper does not include experiments.
   - The authors should answer "Yes" if the results are accompanied by error bars, confidence intervals, or statistical significance tests, at least for the experiments that support the main claims of the paper.
   - The factors of variability that the error bars are capturing should be clearly stated (for example, train/test split, initialization, random drawing of some parameter, or overall run with given experimental conditions).
   - The method for calculating the error bars should be explained (closed form formula, call to a library function, bootstrap, etc.)
   - The assumptions made should be given (e.g., Normally distributed errors).

- It should be clear whether the error bar is the standard deviation or the standard error of the mean.
- It is OK to report 1-sigma error bars, but one should state it. The authors should preferably report a 2-sigma error bar than state that they have a 96% CI, if the hypothesis of Normality of errors is not verified.
- For asymmetric distributions, the authors should be careful not to show in tables or figures symmetric error bars that would yield results that are out of range (e.g. negative error rates).
- If error bars are reported in tables or plots, The authors should explain in the text how they were calculated and reference the corresponding figures or tables in the text.

8. **Experiments compute resources**

   Question: For each experiment, does the paper provide sufficient information on the computer resources (type of compute workers, memory, time of execution) needed to reproduce the experiments?

   Answer: [Yes]

   Justification: It is in Section 3 and Appendix D.

   Guidelines:

   - The answer NA means that the paper does not include experiments.
   - The paper should indicate the type of compute workers CPU or GPU, internal cluster, or cloud provider, including relevant memory and storage.
   - The paper should provide the amount of compute required for each of the individual experimental runs as well as estimate the total compute.
   - The paper should disclose whether the full research project required more compute than the experiments reported in the paper (e.g., preliminary or failed experiments that didn't make it into the paper).

9. **Code of ethics**

   Question: Does the research conducted in the paper conform, in every respect, with the NeurIPS Code of Ethics https://neurips.cc/public/EthicsGuidelines?

   Answer: [Yes]

   Justification: Yes, we followed it.

   Guidelines:

   - The answer NA means that the authors have not reviewed the NeurIPS Code of Ethics.
   - If the authors answer No, they should explain the special circumstances that require a deviation from the Code of Ethics.
   - The authors should make sure to preserve anonymity (e.g., if there is a special consideration due to laws or regulations in their jurisdiction).

10. **Broader impacts**

    Question: Does the paper discuss both potential positive societal impacts and negative societal impacts of the work performed?

    Answer: [Yes]

    Justification: It is in Appendix F.2.

    Guidelines:

    - The answer NA means that there is no societal impact of the work performed.
    - If the authors answer NA or No, they should explain why their work has no societal impact or why the paper does not address societal impact.
    - Examples of negative societal impacts include potential malicious or unintended uses (e.g., disinformation, generating fake profiles, surveillance), fairness considerations (e.g., deployment of technologies that could make decisions that unfairly impact specific groups), privacy considerations, and security considerations.

- The conference expects that many papers will be foundational research and not tied to particular applications, let alone deployments. However, if there is a direct path to any negative applications, the authors should point it out. For example, it is legitimate to point out that an improvement in the quality of generative models could be used to generate deepfakes for disinformation. On the other hand, it is not needed to point out that a generic algorithm for optimizing neural networks could enable people to train models that generate Deepfakes faster.
- The authors should consider possible harms that could arise when the technology is being used as intended and functioning correctly, harms that could arise when the technology is being used as intended but gives incorrect results, and harms following from (intentional or unintentional) misuse of the technology.
- If there are negative societal impacts, the authors could also discuss possible mitigation strategies (e.g., gated release of models, providing defenses in addition to attacks, mechanisms for monitoring misuse, mechanisms to monitor how a system learns from feedback over time, improving the efficiency and accessibility of ML).

11. **Safeguards**

    Question: Does the paper describe safeguards that have been put in place for responsible release of data or models that have a high risk for misuse (e.g., pretrained language models, image generators, or scraped datasets)?

    Answer: [NA]

    Justification: Our work does not involve the described risk.

    Guidelines:

    - The answer NA means that the paper poses no such risks.
    - Released models that have a high risk for misuse or dual-use should be released with necessary safeguards to allow for controlled use of the model, for example by requiring that users adhere to usage guidelines or restrictions to access the model or implementing safety filters.
    - Datasets that have been scraped from the Internet could pose safety risks. The authors should describe how they avoided releasing unsafe images.
    - We recognize that providing effective safeguards is challenging, and many papers do not require this, but we encourage authors to take this into account and make a best faith effort.

12. **Licenses for existing assets**

    Question: Are the creators or original owners of assets (e.g., code, data, models), used in the paper, properly credited and are the license and terms of use explicitly mentioned and properly respected?

    Answer: [Yes]

    Justification: We are the original owners of our assets.

    Guidelines:

    - The answer NA means that the paper does not use existing assets.
    - The authors should cite the original paper that produced the code package or dataset.
    - The authors should state which version of the asset is used and, if possible, include a URL.
    - The name of the license (e.g., CC-BY 4.0) should be included for each asset.
    - For scraped data from a particular source (e.g., website), the copyright and terms of service of that source should be provided.
    - If assets are released, the license, copyright information, and terms of use in the package should be provided. For popular datasets, `paperswithcode.com/datasets` has curated licenses for some datasets. Their licensing guide can help determine the license of a dataset.
    - For existing datasets that are re-packaged, both the original license and the license of the derived asset (if it has changed) should be provided.

- If this information is not available online, the authors are encouraged to reach out to the asset's creators.

13. **New assets**

    Question: Are new assets introduced in the paper well documented and is the documentation provided alongside the assets?

    Answer: [Yes]

    Justification: The code is well documented.

    Guidelines:

    - The answer NA means that the paper does not release new assets.
    - Researchers should communicate the details of the dataset/code/model as part of their submissions via structured templates. This includes details about training, license, limitations, etc.
    - The paper should discuss whether and how consent was obtained from people whose asset is used.
    - At submission time, remember to anonymize your assets (if applicable). You can either create an anonymized URL or include an anonymized zip file.

14. **Crowdsourcing and research with human subjects**

    Question: For crowdsourcing experiments and research with human subjects, does the paper include the full text of instructions given to participants and screenshots, if applicable, as well as details about compensation (if any)?

    Answer: [NA]

    Justification: Not relevant to our work.

    Guidelines:

    - The answer NA means that the paper does not involve crowdsourcing nor research with human subjects.
    - Including this information in the supplemental material is fine, but if the main contribution of the paper involves human subjects, then as much detail as possible should be included in the main paper.
    - According to the NeurIPS Code of Ethics, workers involved in data collection, curation, or other labor should be paid at least the minimum wage in the country of the data collector.

15. **Institutional review board (IRB) approvals or equivalent for research with human subjects**

    Question: Does the paper describe potential risks incurred by study participants, whether such risks were disclosed to the subjects, and whether Institutional Review Board (IRB) approvals (or an equivalent approval/review based on the requirements of your country or institution) were obtained?

    Answer: [NA]

    Justification: Not relevant to this work as we use open dataset.

    Guidelines:

    - The answer NA means that the paper does not involve crowdsourcing nor research with human subjects.
    - Depending on the country in which research is conducted, IRB approval (or equivalent) may be required for any human subjects research. If you obtained IRB approval, you should clearly state this in the paper.
    - We recognize that the procedures for this may vary significantly between institutions and locations, and we expect authors to adhere to the NeurIPS Code of Ethics and the guidelines for their institution.
    - For initial submissions, do not include any information that would break anonymity (if applicable), such as the institution conducting the review.

16. **Declaration of LLM usage**

Question: Does the paper describe the usage of LLMs if it is an important, original, or non-standard component of the core methods in this research? Note that if the LLM is used only for writing, editing, or formatting purposes and does not impact the core methodology, scientific rigorousness, or originality of the research, declaration is not required.

Answer: [No]

Justification: We do not use LLM for any core method development in this research.

Guidelines:

- The answer NA means that the core method development in this research does not involve LLMs as any important, original, or non-standard components.
- Please refer to our LLM policy (https://neurips.cc/Conferences/2025/LLM) for what should or should not be described.